ULTRA LOW NOISE FIBER OPTIC ACOUSTIC SENSOR FOR UNDERWATER APPLICATIONS

A THESIS SUBMITTED TO

THE GRADUATE SCHOOL OF ENGINEERING AND SCIENCE

OF BILKENT UNIVERSITY

IN PARTIAL FULFILLMENT OF THE REQUIREMENTS FOR

THE DEGREE OF

MASTER OF SCIENCE

IN

ELECTRICAL AND ELECTRONICS ENGINEERING

By

Şaban Bilek

August, 2015

ULTRA LOW NOISE FIBER OPTIC ACOUSTIC SENSOR FOR UNDERWATER APPLICATIONS

By Şaban Bilek

August, 2015

We certify that we have read this thesis and that in our opinion it is fully adequate, in scope and in quality, as a thesis for the degree of Master of Science.

Prof. Dr. Ekmel Özbay(Advisor)

Assoc. Prof. Dr. F. Ömer İlday

Assoc. Prof. Dr. Arif Sanlı Ergün

Approved for the Graduate School of Engineering and Science:

Prof. Dr. Levent Onural
Director of the Graduate School

ABSTRACT

ULTRA LOW NOISE FIBER OPTIC ACOUSTIC SENSOR FOR UNDERWATER APPLICATIONS

Şaban Bilek
M.S. in Electrical and Electronics Engineering
Advisor: Prof. Dr. Ekmel Özbay
August, 2015

Fiber optic sensor have many advantages over the conventional sensor technologies such as electromangnetic compatibility, light weight, flexible geometric design, sensing signal at a remote point and no electrical signal at the signal detection point, easy sensor multiplexing,compatibility to fiber optic communication. Experimental studies have been available for underwater acoustic sensor with using fiber optics. In this thesis mandrel type interferometric fiber optic acoustic sensor design is analyzed in terms of noise performance characteristics and design parameters' contribution to noise performance is evaluated.

Acoustic signals create phase change at the fiber optic acoustic probe and phase change is detected by using an interferometer. Experimental setup is used to emulate the design of the sensor and different components are used to evaluate the effect on the noise performance. Phase generated carrier method is evaluated for phase detection method.

Finally noise measurement is done with a experimental setup emulating the design. Noise level is measured around -100 db re rad/$\sqrt{Hz}$ and responsivity of the sensor(-140 dB re rad/μPa) is used to convert noise unit to pressure units and 40 dB re $\mu Pa/\sqrt{Hz}$ noise level in terms of pressure is obtained. This level of noise floor is close to sea sate 0 (SS0) noise level of the ocean. Sea state 0 is the state where there is no wind, wave or shipping traffic. This state is the lowest possible ambient noise available in the ocean and it is quite rare to find such state of the ocean. Therefore self noise of the designed fiber optic acoustic sensor is not the limiting factor for acoustic signal detection. Any signal over the ambient noise of the ocean can be detected using the designed fiber optic acoustic sensor.

Keywords: fiber optic acoustic sensor, interferometric sensors.

ÖZET

SUALTI UYGULAMALARI İÇİN ULTRA DÜŞÜK GÜRÜLTÜLÜ FİBER OPTİK SENSÖR

Şaban Bilek
Elektrik Elektronik Mühendisliği, Yüksek Lisans
Tez Danışmanı: Prof. Dr. Ekmel Özbay
Ağustos, 2015

Fiber optik sensörler geleneksel sensör teknolojilerine göre elektromanyetik uyumluluk, hafiflik, esnek geometrik tasarım, uzak noktada sinyal algılama, sinyal algılama alanında elektriksel bağlantı bulunmaması, sensör çoğullama kolaylığı ve fiber optik iletişim ile uyumluluk gibi birçok avantaja sahiptir. Fiber optik teknolojilerin su altı akustik alanında kullanımına yönelik deneysel çalışmalar mevcuttur. Bu tezde mandrel tipi interferometrik su altı akustik sensörlerin tasarımları gürültü performansı açısından ve tasarım parametrelerinin gürültü performansı üzerindeki etkileri açısından incelenmiştir.

Akustik sinyaller fiber optik prob üzerinde faz değişimi oluşturmaktadır ve faz değişimi interferometre yardımı ile algılanmaktadır. Deneysel bir düzenek ile sensör tasarımı emüle edilmiş ve farklı komponentler kullanılarak gürültü performansı üzerindeki etkileri incelenmiştir. Faz algılama metodu olarak fazda üretilmiş taşıyıcı metodu incelenmiştir.

Son olarak tasarımı emüle eden deneysel bir düzenek ile gürültü ölçümü yapılmıştır. Gürültü seviyesi yaklaşık -100 db re rad/$\sqrt{Hz}$ civarında ölçülmüştür ve sensör hassasiyeti (-140 dB re rad/μPa) kullanılarak gürültü birimi basınca çevrilmiş ve yaklaşık 40 dB re $\mu Pa/\sqrt{Hz}$ gürültü seviyesi elde edilmiştir. Bu seviye deniz durumu 0 (SS0) okyanus ortam gürültü seviyesine yakındır. Deniz durumu 0 seviyesi rüzgar, dalga ve gemi trafiğinin olmadığı durumdur. Bu durumda deniz ortam gürültüsü en düşük seviyededir ve bulunması çok ender bir durumdur. Bu yüzden tasarlanan fiber optik sensörün sinyal algılaması kendi iç gürültüsü ile değil ortam gürültüsü ile sınırlıdır. Ortam gürültüsü üzerindeki herhangibir akustik sinyal tasarlanan fiber optik akustik sensör ile algılanabilir.

Anahtar sözcükler: fiber optik akustik sensör, interferometrik sensörler.

Acknowledgement

It is my pleasure to express my deepest gratitude to my advisor Prof. Dr. Ekmel Özbay for his continuous support, patience, motivation, guidance and understanding throughout my study.

I would like to thank the members of the thesis committee, Assoc. Prof. Dr. F. Ömer İlday and Assist. Prof. Dr. Arif Sanlı Ergün, for being part of my thesis committee.

I would also like to to thank Levent Budunoğlu for his guidance and motivation throughout my study.

I would also like to thank Meteksan Savunma Electrooptic Systems Engineering group, for providing me the lab equipment and devices to use for my thesis. I also would like to acknowledge that my thesis is related to FOAAG (Fiber Optic Acoustic Sensor Development) project of SSM. My work is focused on analyzing the noise performance of the designed sensor. I have used some knowledge that I have acquired during the project for my thesis.

I would also would like to thank my father, my mother and my brother for their endless support throughout my education and professional life. They always have been very understanding and full of moral support.

Finally I would like to thank my lovely wife, Gülbeyaz, and my daughter soon to be born, for their endless support and patience through out my work.

To Gülbeyaz and my daughter...

Contents

1 Introduction **1**

1.1 Organization of Thesis 2

2 Analysis of Self Noise **4**

2.1 Overview of Underwater Fiber Optic Acoustic Sensing 4

2.2 Noise Performance of Interferometric Fiber Optic Acoustic Sensors 11

2.2.1 Interferometer Imbalance 11

2.2.2 Laser Source Phase Noise 14

2.2.3 Laser Source Relative Intensity Noise 15

2.2.4 Detector Noise 16

3 Optical Noise Characterization **17**

3.1 Interferometer Imbalance 17

3.2 Laser Source 19

3.3 Photodetector 21

3.4 Interferometer Type 23

4 Phase Detection Methods 26

4.1 Phase Generated Carrier Method 29

5 Ultra Low Noise Fiber Optic Acoustic Sensors for Underwater Applications 35

6 Conclusion 46

A Code 55

A.1 PGC arctangent method 55

List of Figures

2.1 a) Frustrated total internal refraction b) Lateral misalignment c) Micro bending type of fiber optic acoustic sensors. Arrows shows fiber movement direction due to perturbation 5

2.2 Drum shaped fiber optic acoustic sensor 6

2.3 Mandrel Type Fiber Optic Acoustic Sensor 7

2.4 a) Airbacked Mandrel Type b) Cross section of the mandrel . . . 8

2.5 Mach- Zender interferometer configuration 9

2.6 Michelson interferometer configuration 10

2.7 Interferometer of sensor and reference arm electromagnetic fields . 12

2.8 Coherence of laser after propagating coherence length 14

3.1 Noise Contribution of the Interferometer Imbalance Measurement Setup 18

3.2 Noise Contribution of the Interferometer Imbalance 19

3.3 Noise Contribution of the Laser Source 20

3.4 Noise Contribution of Detector 22

3.5 Mach-Zender interferometer noise measurement setup 23

3.6 Michelson interferometer noise measurement setup 24

3.7 Noise Contribution of the Interferometer Type 25

4.1 Interferometric output with phase bias ϕ_e and small signal phase change $\delta\phi$ 27

4.2 Phase compensation in Mach-Zender interferometer 28

4.3 Phase Generated Carrier- Arctangent Algorithm 31

4.4 Fringe Counting for Correcting Large Phase Signals 32

4.5 Random phase signal and demodulated phase signal with PGC method 33

4.6 Spectrum of detector output 34

5.1 Spectral noise levels and noise sources in the ocean 36

5.2 Noise Measurement Setup 41

5.3 Picture of the Noise Measurement Setup 42

5.4 Noise Level of the Designed Fiber Optic Acoustics 43

5.5 Phase amplitude linearity 44

5.6 Phase amplitude linearity with frequency change 45

List of Tables

3.1 Laser Source Parameters 20

3.2 Detector Parameters 21

5.1 Sea state, wind speed and wave height 37

5.2 Frequency, wavelength and maximum usable range 39

5.3 General usage of sound spectrum 40

Chapter 1

Introduction

Over the past few decades telecommunication industry has experienced a big leap and become more reliable with higher performance and lower price. Fiber optic communication has been leading the revolution of telecommunication industry. Consequently, there has been excessive investment and research focus on fiber optics and optoelectronics, which has resulted mass production of various fiber optic and optoelectronic components. Fiber optic sensor technology has benefited from the improvement of fiber optic communication technology, because most of the components used and technological developments are overlapping with fiber optic communication technology and both technologies are feeding each other.

Fiber optic sensors have major advantages over the conventional sensors, such as light weight, flexible geometric design, electromagnetic interference immunity, no electrical connection at the sensing point, compatible with fiber optic communication, easy to multiplex. Underwater acoustic sensing, strain sensing, rotation sensing (gyroscopes), chemical/biomedical sensing, temperature sensing are the main areas in which fiber optic sensor technology has successful sensors. [1]

Application examples of fiber optic sensors are as follows: Strain sensors used to monitor structure health of the buildings, bridges, tunnels, dams, pipelines. These sensors are used for early warning system to prevent major failure of the structure. [2, 3, 4, 5] Acoustic, vibration and pressure sensors are used in down hole oil and gas explorations [6, 7, 8], seabed and towed military surveillance [9, 10], medical applications such as ultrasound and blood pressure measurement [11, 12, 13]. Temperature sensors are used in monitoring transformer, power cables and transmission lines [14, 15], detecting oil and gas leakage in pipelines [16, 17, 18]. Gas, chemical and particle sensors are used for detecting gases and chemical like methane, carbon dioxide, ammonia, chloroform [19, 20, 21]. Inertial sensors are used for navigation, control and guidance systems in robots, cars, missiles and aircraft and helicopters [22, 23, 24].

Fiber wounded hydrophone type sensors was one of the first applications for underwater fiber optic sensor applications. In the 1980s first field trials have been done for hydrophone type of sensors. Array of hydrophones are used as hull sensor on submarines for surveillance systems and linear arrays are used as towed arrays and for harbour protection systems. [25]

1.1 Organization of Thesis

In this work noise analysis of a mandrel type underwater fiber optic acoustic sensor has been done, parameters effecting the performance is analyzed. Experimental work has been done to support theoretical work and a recipe has been developed to design ultra low noise underwater fiber optic sensors.

In chapter 2, background for mandrel type hydrophone type of underwater fiber optic sensors is given.

In chapter 3, experimental results are given to evaluate the design components of a mandrel type fiber optic acoustic underwater sensor. Experimental setups are installed to emulate the sensor design and by changing the components of the design one by one effects on the noise performance is evaluated.

In chapter 4, phase detection method is given. PGC (Phase Generated Carrier) method will be analyzed. Using MATLAB, PGC method will be modeled and this model will be analyzed.

In chapter 5, noise sources available in the ocean and noise levels of the ocean are analyzed. Noise performance of the designed fiber optic acoustic sensor is evaluated by measuring noise level of en experimental setup emulating the design. Noise performance of the designed fiber optic sensor is evaluated comparing with noise levels of the ocean.

In chapter 6, performance of designed sensor will be evaluated. Possible operational scenarios will be discussed.

Chapter 2

Analysis of Self Noise

2.1 Overview of Underwater Fiber Optic Acoustic Sensing

Fiber optics sensors have been used in military and seismic applications. Mandrel type fiber optic acoustic sensors have successful examples in oil industry to monitor seismic motions in oil bed reservoirs [26]. Properties such as easy multiplexing and remote sensing enables fiber optic hydrophones to be tailored in arrays covering km's range and these sensor arrays are used as surveillance systems for protecting ports and harbours, offshore facilities from terrorist activities. Fiber optic hydrophone type of sensors have succesful use in military applications as towed arrays which is used in harbour protection.[27] Flexible geometrical design enables fiber optic sensor to be use in different tactical scenarios, one good example of this is the hull array sonar used in Virginia Class Submarine [28]

Fiber optic acoustic sensors can be classified in two main groups, intensity detection based sensors and phase detection based sensors. Intensity based sensors generally composed of a mechanical/optical design, in which perturbation caused by the acoustic signal changes the coupling efficiency of the light that is passing through or reflected from the sensor and light intensity detected from the sensor

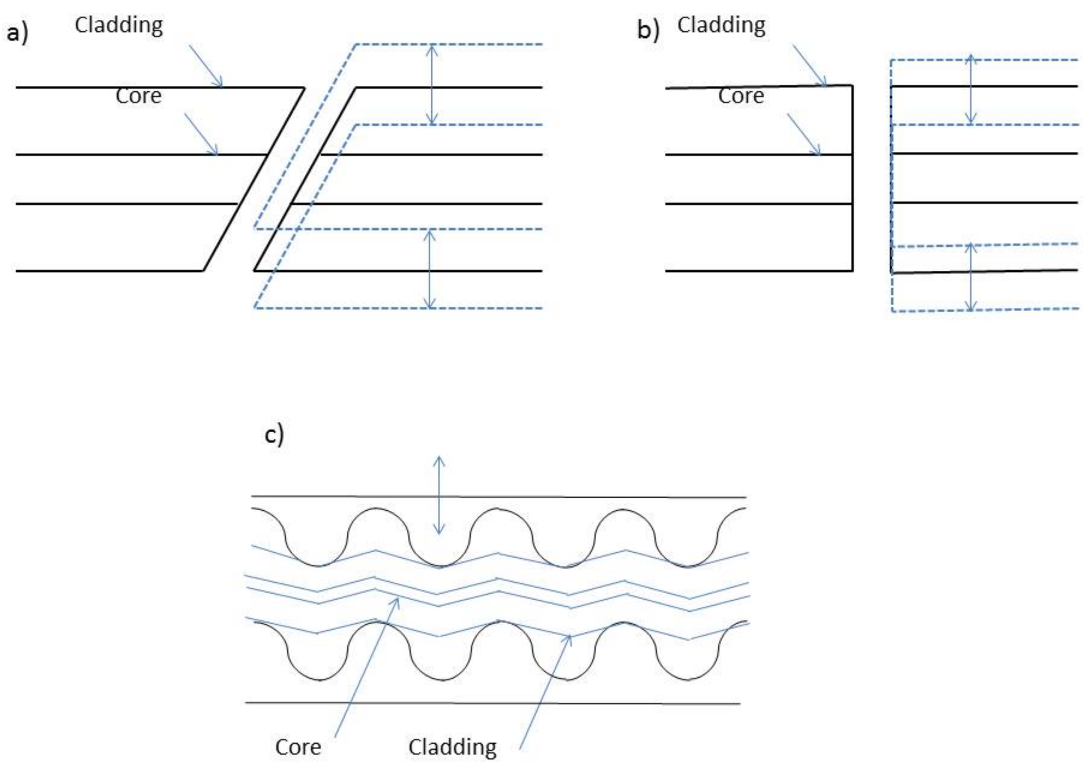

Figure 2.1: a) Frustrated total internal refraction b) Lateral misalignment c) Micro bending type of fiber optic acoustic sensors. Arrows shows fiber movement direction due to perturbation

changes. Frustrated total internal refraction, lateral misalignment, micro bending type of sensors can be given example for intensity based fiber optic acoustic sensors. [29] Since the intensity based fiber optic sensors works on a loss mechanism, they are limited with the minimum optical power that can be detected and in order to have a very high sensitive sensor, very small optical powers have to be detected, because of dynamic range and the sensitivity of the intensity based fiber optic sensors are limited with the detector that is used and their performance is not as good as the phase detection based fiber optic acoustic sensors.

Phase detection based fiber optic acoustic sensors detects acoustic signals by strain generated by the pressure change on fiber optic cable. Strain on fiber optic cable cause refractive index change and physical length change. As a result optical path and phase of the light passing through the fiber changes. In this work I will concentrate on phase detection based fiber optic acoustic sensors. Fractional phase change in fiber optic sensors due to pressure change ΔP is given as;

$$\frac{\Delta\phi}{\phi\Delta P} = \frac{1}{\Delta P}\left(\varepsilon_z - \frac{n_{eff}^2}{2}[\varepsilon_r(p_{11}+p_{12})+\varepsilon_z p_{12}]\right) \tag{2.1}$$

where ε_z and ε_r are axial and radial component of strain, p_{11} and p_{12} are the Pockel's coefficients, ϕ=n_{eff}kL is the total phase, $k = \frac{2\pi}{\lambda}$, λ is the wavelength and L is the fiber length. First term in the equation represents the contribution from the length change of the fiber and the second term represents the contribution coming from the refractive index change caused by the elastooptic effect. [30]

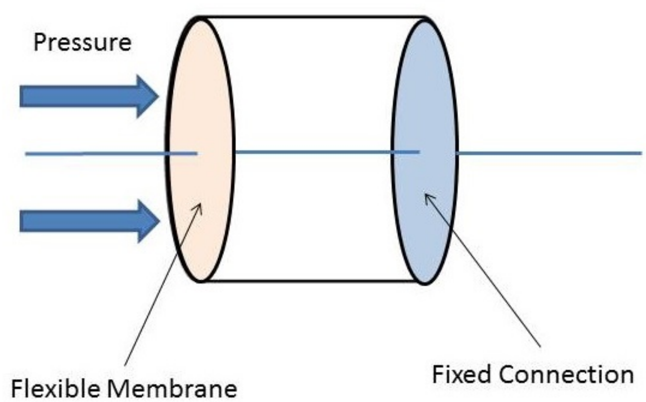

Figure 2.2: Drum shaped fiber optic acoustic sensor

In order to amplify the responsivity of the sensor there are two common approaches. First one is to amplify the strain by a mechanical encapsulation on the sensing fiber. Drum like structures are used to amplify the strain on sensing fiber. One end of the drum is fixed and the other has a flexible membrane and the sensing fiber passes through the drum. As the pressure change on the drum, membrane moves back and forth pulling the sensing fiber and exerting strain on sensing fiber. There is a trade of in this type of sensors, using large membrane to increase responsivity of the sensor, decreases the mechanical resonance of the flexible membrane to very low frequencies. At frequencies higher than the resonance frequency responsivity of the sensor drops dramatically. Hence it is difficult to have wide bandwidth high sensitivity sensors with drum configuration.

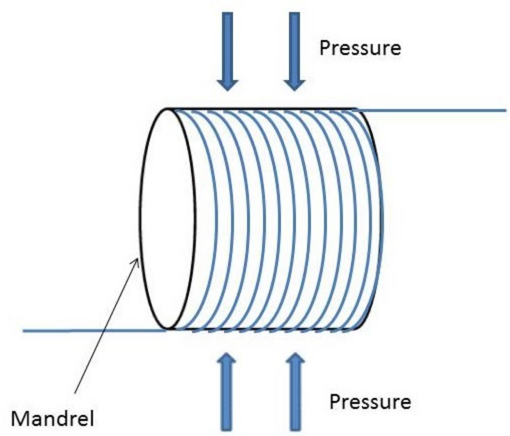

Figure 2.3: Mandrel Type Fiber Optic Acoustic Sensor

Other approach to increase the responsivity of the fiber optic acoustic sensor is to increase the length of sensing fiber. Mandrel type of sensors are good example of this approach. Sensing fiber is wound on a solid mandrel. As the pressure on the mandrel changes, mandrel does the breathing motion and radially extends and contracts. Breathing motion exerts strain on sensing fiber. As the length of the fiber wound on mandrel increases responsivity of the sensor increases, but you can not increase radius and length of the mandrel to increase the fiber winding area, this will decrease the mechanical resonance. Size of the mandrel is limited by the detection bandwidth. Resonance frequency should be higher than the maximum detection frequency. Winding fiber more than one layer is one way to increase fiber length but, as the fiber layer on the mandrel increases, mandrel becomes more stiff and breathing motion is restricted. As a result the responsivity of the sensor decreases.

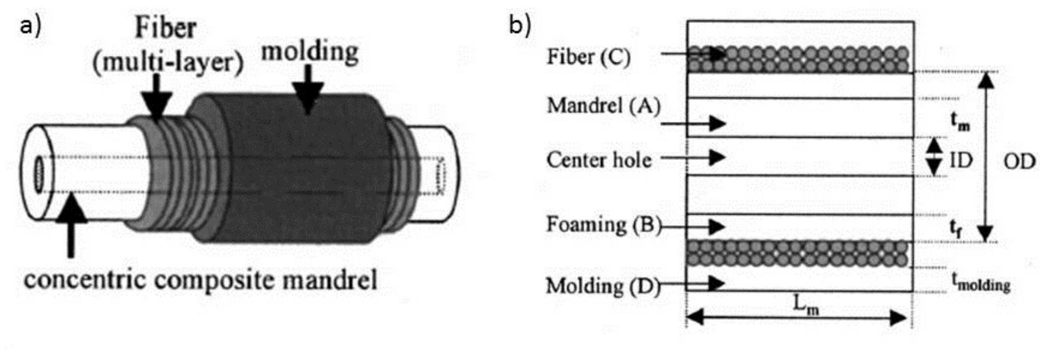

Figure 2.4: a) Airbacked Mandrel Type b) Cross section of the mandrel

Mechanical design of the sensor and Young's modulus of the material determines the resonance frequency of the mandrel and deflection of the mandrel against the pressure change, therefore the responsivity of the fiber optic sensor. Youngs modulus defines the elasticity of the material, therefore having a low Young modulus results high sensitivity. Putting a concentric hole inside the mandrel increases the deflection against the pressure change but in return robustness of the sensor decreases and under deep water conditions because of the high static pressure mandrel may get structurally damaged and collapse. Without compromising the robustness of the sensor, a foaming layer with low Young modulus is used over a stiff mandrel and the responsivity is increased with the flexibility of the foaming layer and the integrity of the of the sensor is ensured with the stiff mandrel. Sensing fiber wound on the mandrel has to be protected from the corrosion of the sea water, for that purpose a whole sensor should molded with a thin polymer layer which is compliant with the sensor and should not decrease the sensitivity of the fiber optic sensor. Design of the sensor mandrel is composed of first selecting mandrel, foaming and molding layer materials and then determining the mechanical dimensions such as length of the mandrel, inner and outer diameter of the mandrel which specifies the resonance frequency of the sensor. By optimizing the design parameters maximum deflection of the mandrel structure against pressure change is obtained for a specific detection bandwidth. Breathing motion of the mandrel stretches the sensing fiber wound on the mandrel resulting phase change of the laser passing through the fiber. Responsivity of the fiber optic acoustic sensors are generally defined in dB re 1 rad/μPa unit and by increasing the responsivity of the sensor, higher phase change will be obtained for the same pressure change. [31, 32]

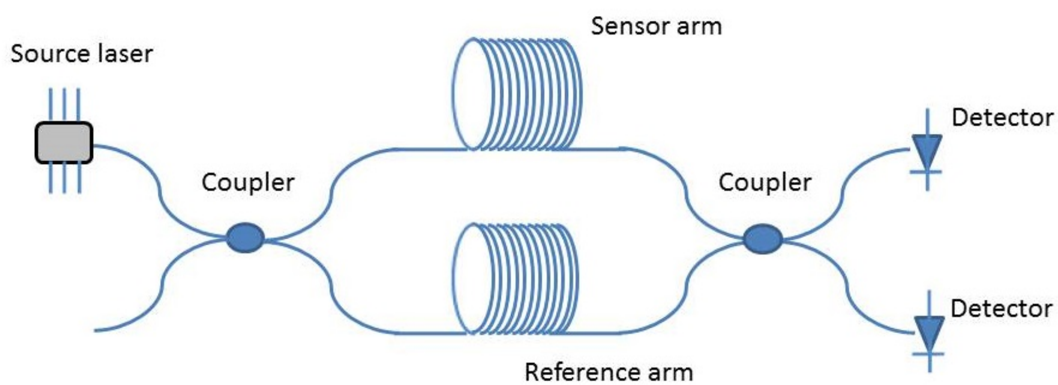

Figure 2.5: Mach- Zender interferometer configuration

Phase change in laser passing through the fiber can not be detected directly since photodetectors with 10^{14} Hz bandwidth does not exist. In order to detect the phase change caused by the acoustic signal an interferometer with the same length reference arm is used to convert phase change to intensity modulation. One arm of the interferometer is isolated from the acoustic signal and mixed with the sensing arm and phase difference between the reference and the sensing arms converted into intensity modulation by the interferometer. Michelson and Mach-Zender interferemeters commonly used. Michelson interferometer uses one coupler which divides the laser source in two arms, sensor and reference arms. Laser passing through the sensor and reference arms reflected from the mirrors and transverse the same path than mixed at the coupler and directed to the detector. Same coupler is used for both dividing and recombining the laser. Mach-Zender interferemoter uses two couplers one for dividing the signal and the second coupler is used for combining the lasers coming through the sensor and reference arms.

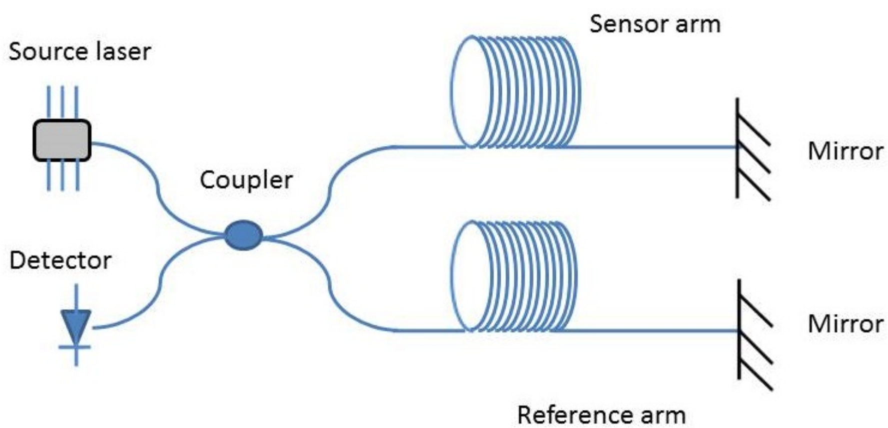

Figure 2.6: Michelson interferometer configuration

Combined signals directed to detectors. Laser transverse in forward direction in Mach-Zender interferometer, whereas in Michelson interferometer laser transverse in both forward and backward directions. Michelson interferometers looks like the folded version of Mach-Zender interferometer and in terms of optical loss budget they are similar, however there are differences. Michelson interferometer uses one coupler less than the Mach-Zender interferometer and it is physically easier to package. Due to the fact that laser passes twice from both reference and sensor arms optical phase shift due to the acoustic signal is doubled. Michelson interferometer configuration depends on the reflection mechanism, therefore it is sensitive to other reflections such as Rayleigh scattering induced back reflections and forms unintended interference which significantly contributes to noise of the system. On the other hand Mach-Zender interferometer has more components and lower responsivity compared to Michelson interferometer, but it is immune to scattering mechanisms in terms of noise performance since laser transverse only in forward direction in Mach-Zender interferometer configuration.

Performance of a sensor can be evaluated in terms of responsivity, noise performance and dynamic range. Responsivity of the phase detection based underwater acoustic sensors determined by the optomechanical design of the sensor head as given above. Dynamic range of a sensor is determined by the minimum and maximum acoustic signal levels that can be detected. Minimum detectable pressure level is determined by both responsivity and the noise performance of the sensor.

$$MinimumDetectablePressure\left(\mu Pa/\sqrt{Hz}\right) = \frac{SystemNoiseLevel\left(rad/\sqrt{Hz}\right)}{Responsivity\,(rad/\mu Pa)} \tag{2.2}$$

2.2 Noise Performance of Interferometric Fiber Optic Acoustic Sensors

In this work, noise performance of an interferometric fiber optic acoustic sensor will be analyzed, this type of sensors are composed of an interferometer, laser source, photodetectors and sensor probe. Effects of the parameters such as phase noise of the laser source, relative intensity noise of the laser source, interferometer imbalance, and detector noise will be analyzed in the preceding sections.

2.2.1 Interferometer Imbalance

Monochromatic light can be modeled as a scalar wave $\psi(r,t)$ where it is a function of time, t and spatial position r. Electric field and magnetic field components of light satisfies the following scalar wave equation derived from Maxwell's equations.

$$\bigtriangledown^2\psi\,(r,t) = \frac{1}{c^2}\frac{\delta^2\psi\,(r,t)}{\delta t^2} \tag{2.3}$$

where $\bigtriangledown^2$ is the Laplacian operator and c is the speed of light. Any function that satisfies the above equation can represent optical waves. Light propagating through a single mode fiber can be modeled as a monochromatic plane wave for the sake of simplicity and it is mathematically represented as,

$$\psi\left(\vec{r},t\right) = E_0 exp\left(i\left(\vec{k}.\vec{r} - 2\pi\upsilon t\right)\right) \tag{2.4}$$

where E_0 is the amplitude of the field, $\vec{k}$ is the propagation wave vector and υ is the frequency of the light. Assume planar wave is propagating in z direction, wave function simplifies and becomes $E_0 exp\left(i\left(kz - wt\right)\right)$ where $w = 2\pi\upsilon$ is the angular frequency of the light. [33]

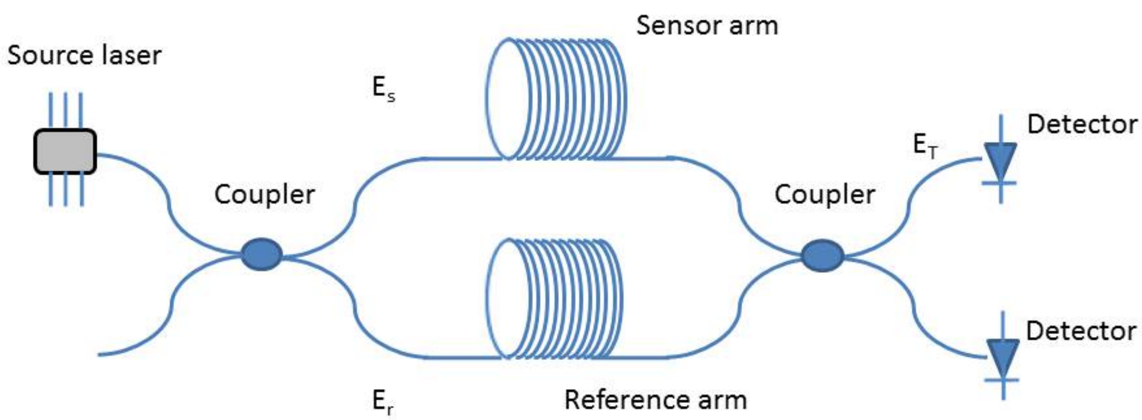

Figure 2.7: Interferometer of sensor and reference arm electromagnetic fields

Interference of light propagating through the reference arm and sensor arm can be given as;

$$E_t = E_s exp\left(i\left(kL_s - wt + \phi_s\right)\right) + E_r exp\left(i\left(kL_r - wt + \phi_r\right)\right) \tag{2.5}$$

where E_s, E_r are the amplitude of the electromagnetic field in sensor arm and reference arm, L_s and L_r are the length of sensor arm and reference arm of the interferometer and ϕ_s and ϕ_r are the phase changes of sensor and reference arms. Photodetectors can only detect the intensity of light since the frequency of the light is very high. The intensity of the light is proportional to time averaged value of the squared electric field. $I\alpha\langle E.E^*\rangle$. Intensity of the light detected at the detector can be calculated as below.

$$I_T = \langle\left(E_s + E_r\right).\left(E_s + E_r\right)*\rangle = \mid E_s \mid^2 + \mid E_r \mid^2 + 2Re\left(E_s E_r^*\right) \tag{2.6}$$

$$= \mid E_s \mid^2 + \mid E_r \mid^2 + 2 \mid E_s \mid\mid E_r \mid cos\left(\phi_s - \phi_r + k\left(L_s - L_r\right)\right) \tag{2.7}$$

The light intensity at the output of the interferometer is not addition of intensities coming from sensing arm and reference arms. Reference arm of the fiber optic sensor is used to balance the interferometer and isolated from the acoustic signal, therefore we assume that ϕ_r=0, there is no phase change due to acoustic signals in reference arm. The intensity at the output of the interferometer is given as,

$$I_T = I_s + I_r + 2\sqrt{I_s I_r} cos\left(\phi_s + k\left(\Delta L\right)\right) \tag{2.8}$$

where ΔL is the difference of the sensing arm length and the reference arm length. As it can be seen from the above expression path imbalance has role in the interferometer output. When we look at the expression above, path imbalance term is added to the phase signal coming from sensing arm of the interferometer. Therefore, we can interpret that path imbalance directly effects the phase noise of the interferometric fiber optic acoustic sensor.

2.2.2 Laser Source Phase Noise

Although the laser sources are known as single frequency light sources, they do have certain linewidth (lw) which results the corruption of phase coherence of the photons leaving the laser after propagating a certain distance. The distance in which the phase coherence is substantially preserved is defined as the coherence length. Coherence length is calculated as,

$$L_{coherence} = c\tau_{coherence} = \frac{c}{\pi lw} \tag{2.9}$$

where c is the speed of light and $\tau_{coherence}$ coherence time. Depending on the linewidth of the laser coherence length can change dramatically.

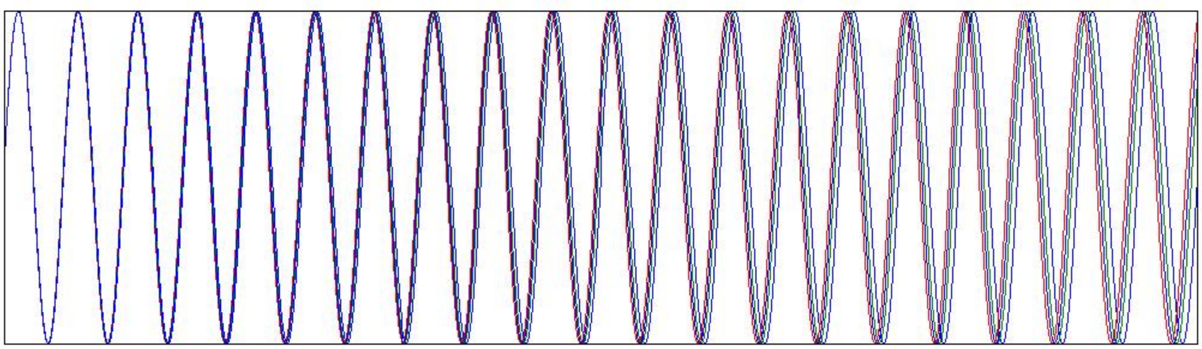

Figure 2.8: Coherence of laser after propagating coherence length

Laser phase noise is due to the fluctuations of optical phase. As it can be seen from the coherence schematic above, linewidth of the laser is one of the reason for phase noise. Linewidth and the laser phase noise used as if they represent the same thing, but in reality linewidth of the laser is determined by the low frequency component of the phase noise. In many cases linewidth is given as the phase noise of the laser, but in some applications complete phase noise spectrum of the laser is used. [34] In two beam interferometers noise power at the output of the interferometer is proportional to the coherence time of the laser source. [35] Therefore noise of an interferometric fiber optic sensor is directly effected from the linewidth of the laser source, or phase noise of the laser source.

2.2.3 Laser Source Relative Intensity Noise

Relative intensity noise(RIN) is the term defining the intensity flactuations of the laser source. It is defined as variation of the power normalized to the average power. The optical power of a laser source can be define as;

$$P(t) = \bar{P} + \delta P RIN = \frac{\delta P}{\bar{P}} \tag{2.10}$$

$$RIN = \frac{\delta P}{\bar{P}} \tag{2.11}$$

average power and a zero mean δP fluctuating around the average power. Statistical description of the relative intensity noise is defined as the Fourier transform of the aotucorrelation of the intensity noise which gives a power spectral density as a function of frequency.

$$S(f) = \frac{2}{\bar{P}^2} \int_{-\infty}^{\infty} \langle \delta P(t) \, \delta P(t+\tau) \rangle \, exp(i2\pi f\tau) d\tau \tag{2.12}$$

The units of power spectral density of the RIN is in Hz^{-1}, generally it is also given in logarithmic units as dBc/Hz. Datasheets of the commercial products commonly gives root mean square RIN parameter which is the square root of the power spectral density integrated over an interval of $[f_1, f_2]$.

$$RIN_{\mathrm{rms}} = \frac{\delta P}{\bar{P}}_{rms} = \sqrt{\int_{f_1}^{f_2} S(f) \, df} \tag{2.13}$$

In fiber optic sensing, interferometers are used to convert phase change to intensity modulation. Phase change is demodulated from the intensity by using different methods. Laser intensity noise adds noise to intensity modulation at the output of the interferometer and spoils the demodulated phase term. Therefore, having a lower laser intensity noise will improve the noise performance of a fiber optic interferometric sensor.

2.2.4 Detector Noise

Photodetector noise is composed of shot noise, dark current and thermal noise but commercial products gives noise equivalent power (NEP) parameter to represent the noise of the photodetectors. When there is no light illuminated on the detector, the optical power value that makes SNR one is defined as the NEP parameter. NEP parameter is calculated as,

$$NEP = \frac{i_{noise}}{R} \tag{2.14}$$

where, i_{noise} is the spectral current noise at the output of the detector when there is no light illuminated and R is the responsivity of the photodetector. The unit of NEP is given as W/$\sqrt{Hz}$.

Photodetector is used to convert optical signal to electrical signal. During this conversion, detector noise is added to electrical signal representing the output of the interferometers. This electrical signal is used to demodulate the phase change caused by the sensing unit of the fiber optic acoustic sensor. Therefore, choosing a detector with lower NEP value will improve the noise performance of the fiber optic acoustic sensor.

Chapter 3

Optical Noise Characterization

In this chapter, experimental setups will be constructed to compare the effects of the design parameters on the noise performance of the fiber optic acoustic sensors. For this purpose complete sensor system will not be constructed but similar experimental systems will be constructed emulate the sensor system and effects of the design parameters will be analyzed.

3.1 Interferometer Imbalance

Interferometer imbalance is one of the parameters that is effecting the noise of an interferometric fiber optic acoustic sensor. In order to analyze effect of the interferometer imbalance the below experimental setup is constructed. As the laser source PS-NLL model numbered product of Teraxion is used. It is a narrow linewidth ($\leq 5kHz$) laser source with center wavelength at 1550nm. At the output of the laser source an isolator is used to block the back reflections that can spoil the stability of the laser. VOA (variable optical attenuator) is used to adjust the power level for preventing detector saturation. Mach-Zender type interferometer is used, and two 50/50 coupler is used to construct the interferometer. First coupler is used to divide laser source in two arms and the second coupler is used

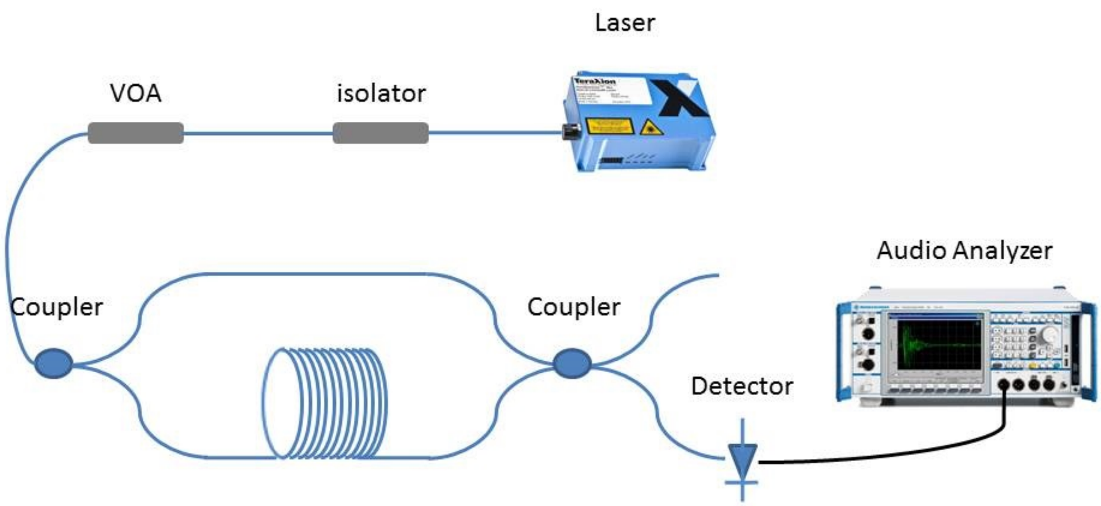

Figure 3.1: Noise Contribution of the Interferometer Imbalance Measurement Setup

to combine the lasers coming from sensor and reference arms. At the output of the interferometer PDB410C fixed gain balanced amplified photodetector of the Thorlabs company is used to convert the optical power to voltage.

Noise of the interferometer is analyzed with using UPV audio analyzer of Rohde Schwarz, FFT of the signal is calculated by the audio analyzer. FFT bandwidth of the audio analyzer is set to 22 kHz and FFT length is set to 16k. Fiber length used for the sensor arm and the reference arm set to equal length, than fiber is added to one arm of the interferometer to add imbalance. Noise performance of the measurement system is compared for different imbalance lengths. Noise measurements are taken when the interferometer arms are equal and when the interferometer is not balanced. In order to observe the effect of imbalance to noise level of the system 2m, 5m, 10m, 15m, 44m fiber added to one arm of the interferometer and noise measurements are taken for each imbalance without changing laser source, power level of the laser source and the detector.

As it can be seen from the measurements, noise of the system increases as the imbalance of the interferometer increases, therefore it is essential to have the

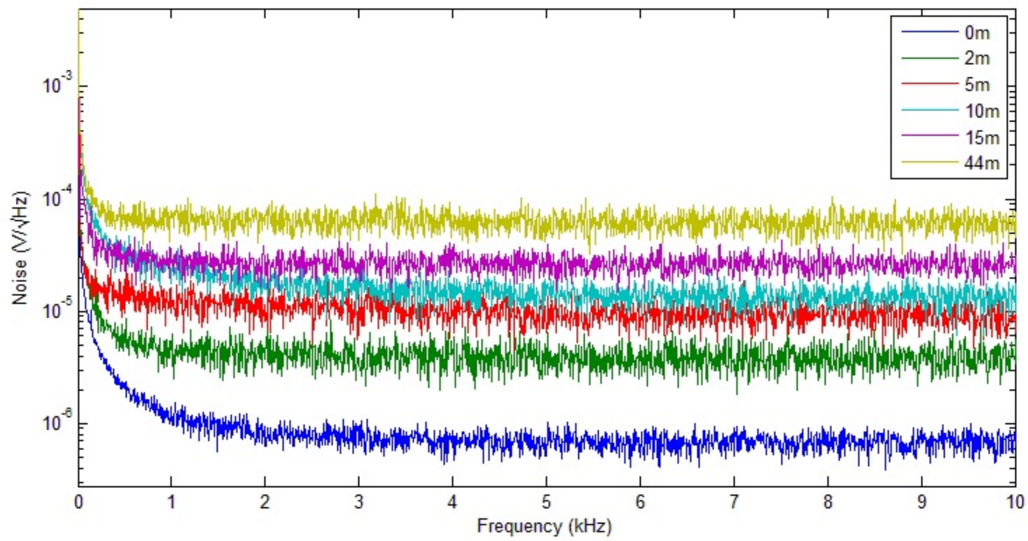

Figure 3.2: Noise Contribution of the Interferometer Imbalance

imbalance of the interferometer as small as possible. For this purpose a reference mandrel is used to balance the interferometer and same length of fiber is wound over the reference mandrel. Responsivity of a mandrel type fiber optic acoustic sensor is increased by increasing the fiber length wound over the sensing mandrel. Assuming 44m fiber is used for the sensing mandrel, if a reference mandrel is not used to balance noise floor of the sensor system increases from $10^{-6}V/\sqrt{Hz}$ to $10^{-4}V/\sqrt{Hz}$ meaning 40dB increase in the noise floor.

3.2 Laser Source

Laser source used in the fiber optic acoustic sensor is effecting the noise performance of the sensor system because of the phase noise and RIN of the laser. Since it is impossible to tune phase noise and RIN parameters of a laser, I have used three different laser sources to see the effect on the noise floor of the system. First one is PSL-450 from Princeton Lightwave company, which has the

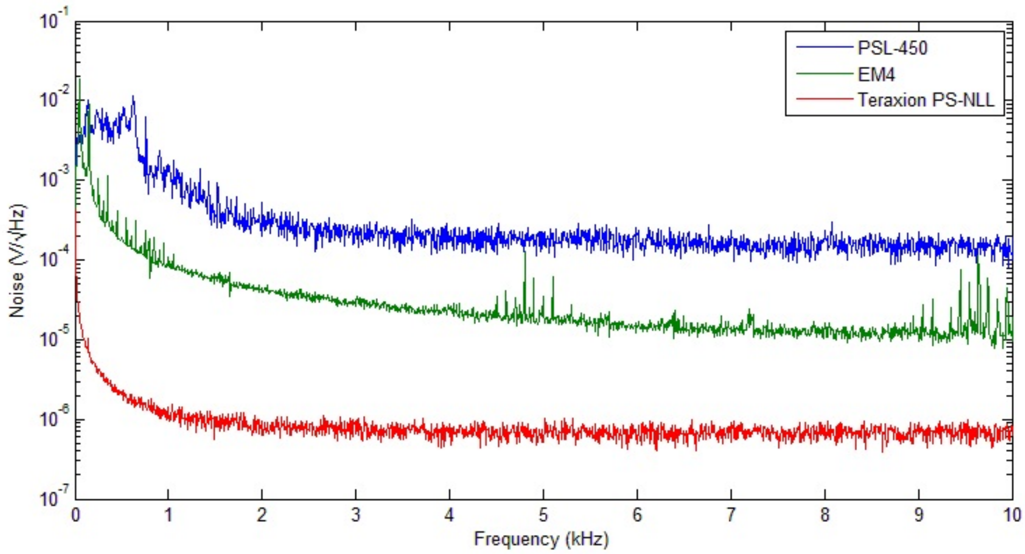

Figure 3.3: Noise Contribution of the Laser Source

worst linewidth value 12nm corresponding to approximately 1.5THz. Second laser source is the EM4 high power DFB laser of the Gooch&Housego company which has low RIN value (-150dBc/Hz) and 1Mhz linewidth. Third laser source is Pure Spectrum-Narrow Linewidth Laser (PS-NLL) of the Teraxion company which has very narrow linewidth, 5kHz, and RIN value of this laser is -130dBc/Hz. Parameters of the lasers can be seen at the table.

Table 3.1: Laser Source Parameters

	PSL 450	EM4 DFB Laser	Teraxion PS-NLL
RIN	-	-150dBc/Hz	-130dBc/Hz
Linewidth	1.5 THz	1Mhz	5kHz

Measurements are taken with balanced Mach-Zender interferometer and for each laser source and power levels are set to the same level at the output of the interferometer by using variable optical attenuator. At the output of the interferometer PDB410C fixed gain balanced amplified photodetector of the Thorlabs company is used and noise of the setup is measured with UPV audio analyzer. As it can be seen from the Figure 3.3 quality of the laser source is effecting the system noise performance. Worst noise measurement is taken with PSL- 450 laser. This laser has 12nm linewidth and RIN parameter is not given for this laser. Best noise performance is taken with low linewidth PS-NLL laser, which has the lowest linewidth value. It is obvious that the laser source is effecting the noise performance of fiber optic acoustic sensors. It can be interpreted that having a lower linewidth laser source results lower noise floor, but it is difficult to interpret the effect of the RIN of the laser source on the noise performance of the sensor system. In order to analyze the effect of RIN on the noise performance of fiber optic acoustic sensors, measurement with different laser sources having similar linewidth and different RIN values should be taken. What we have learned from these measurements is that laser source with low linewidth should be used to get low noise performance underwater fiber optic acoustic sensors.

3.3 Photodetector

Photodetector used in the fiber optic acoustic sensor is the part where the laser intensity is converted into electrical signals, since the bandwidth of the current detector technology is not enough to catch the phase change, interferometers are used to convert the phase change into intensity modulation. Commercial detectors have NEP (noise equivalent power) value in their datasheet to represent the noise performance and responsivity values to conversion gain from light intensity to voltage.

Table 3.2: Detector Parameters

	Newport 1617-AC-FS	Thorlabs PDB410C	Thorlabs SIR5
NEP	20pW$\sqrt{Hz}$	3.8pW$\sqrt{Hz}$	2fW$\sqrt{Hz}$
Responsivity	700V/W	50 x 10^3V/W	50V/W
Bandwidth	800MHz	100MHz	5GHz

In order to evaluate the effect of the photo detector on the noise performance of the fiber optic acoustic system, the measurement setup at Figure 3.1 is used. A balanced Mach-Zender interferometer is used and as the laser source PS-NLL laser of the Teraxion company is used. Noise of the system is measured with UPV audio analyzer of the Rohde&Schwarz company and FFT parameters are the same as before. Three different photodetectors are used and noise measurements are taken for each detector. First detector is the balanced InGaAs PIN detector with fixed gain, Newport 1617-AC-FS, of Newport company, which has 800MHz bandwidth, 700V/W responsivity and 20pW$\sqrt{Hz}$ NEP. Second detector is the PDB410C of the Thorlabs company. This detector is an amplified InGaAs PIN detector with 100MHz bandwidth, 50 x 10^3V/W responsivity and 3.8pW$\sqrt{Hz}$ NEP. Third detector is SIR5 InGaAs PIN detector of the Thorlabs company, which has 5GHz bandwidth, 50V/W responsivity and 2fW$\sqrt{Hz}$ NEP. This detector does not have an amplifier but 50 ohm termination and it is powered from a battery.

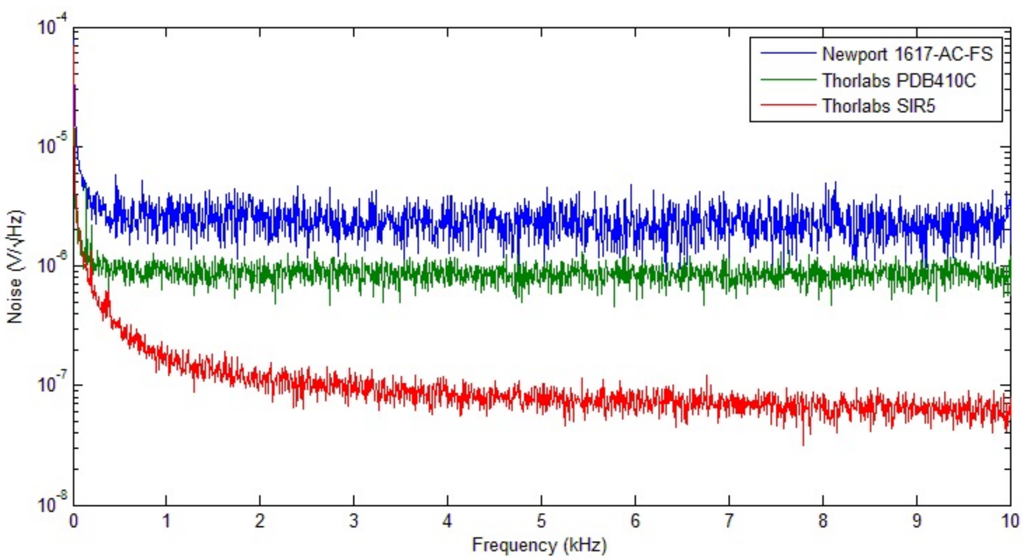

Figure 3.4: Noise Contribution of Detector

Measurement results shows that the NEP value of the detector is determining the noise floor of the fiber optic acoustic sensor, with the same measurement setup lower NEP parameter results lower noise floor. One has to notice that NEP value is given as noise spectral density, NEP value is multiplied with the square root of the bandwidth to calculate noise of the detector. Using higher bandwidth than the required bandwidth results extra noise. When we look at the noise measurements SIR5 has the lowest noise floor, however it is not an amplified detector and responsivity of the detector is lower than the other detectors. Since the responsivity is lower, more optical power is needed to obtain the same voltage level. Noise level obtained with SIR5 detector is quite low, it can be detected with an audio analyzer, but with a standard electronic circuit you should either add an amplifier circuit to increase the voltage level which will add extra noise, or optical power should be increased.

In order to have the optimum performance for a fiber optic acoustic sensor system, detector with minimum NEP value and maximum responsivity should be used and the bandwidth of the detector shouldn't be more than the required bandwidth.

3.4 Interferometer Type

One main part of the fiber optic acoustic sensor is the interferometer that is used to convert phase change of the laser in to intensity modulation. Mach-Zender and Michelson interferometers are two common interferometer types that are used in the fiber optic acoustic sensor design.

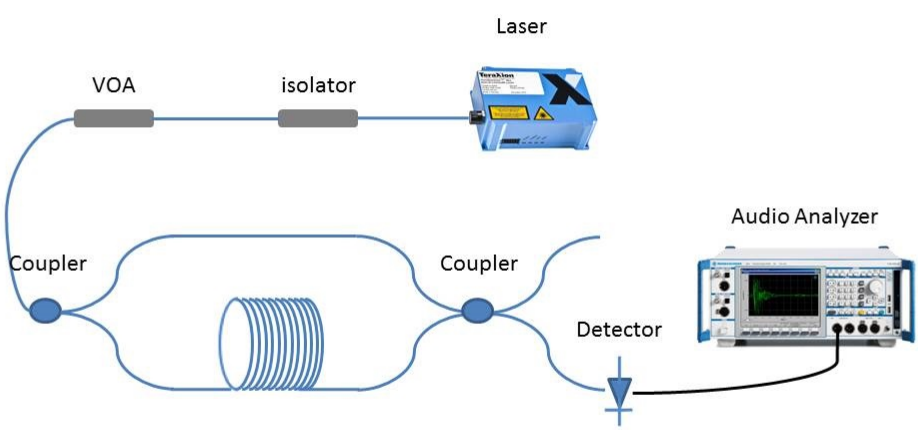

Figure 3.5: Mach-Zender interferometer noise measurement setup

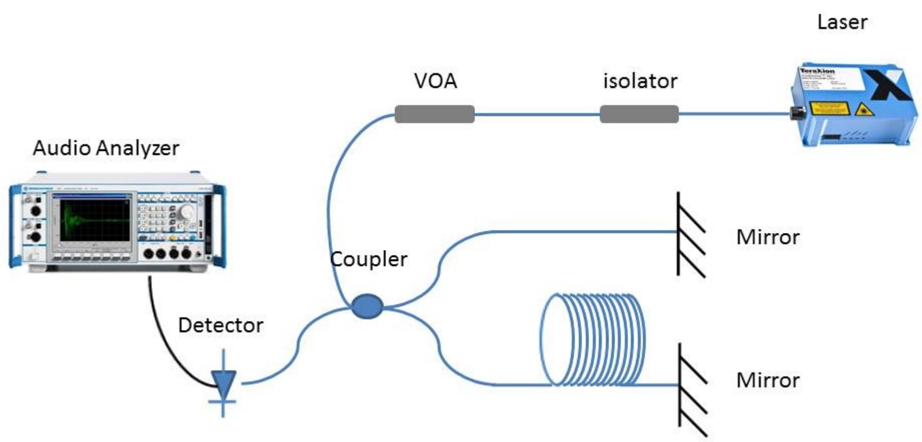

Figure 3.6: Michelson interferometer noise measurement setup

Schematic figures for Michelson and Mach-Zender noise measurement setups are seen above. In both measurement setups, PS-NLL laser source of the Teraxion company is used and PDB410C fixed gain balanced amplified photodetector of Thorlabs is used as the detector. Noise measurements are taken with UPV audio analyzer of the Rohde&Schwarz, and FFT bandwidth is set to 22kHz and FFT length is set to 16k for both noise measurements. For both interferometer systems power levels reaching to the detector is adjusted to the same level.

Michelson interferometer seems like the folded version of the Mach-Zender interferometer, the laser on the both sensor and reference arms are reflected back and mixed with same coupler that divides the laser in two arms. Because of this, laser travels the same path twice and physical length of the imbalance is multiplied by two for Michelson interferometer. Therefore, adding 1m of fiber length to one arm results 2m imbalance at the interferometer. Michelson interferometer depends on the reflection of the laser in both arms, therefore it is sensitive to other reflections such as impurity, Rayleigh induced back scattering and these reflections become extra noise sources for the system.

Mach-Zender interferometer has forward laser propagation, hence it is more

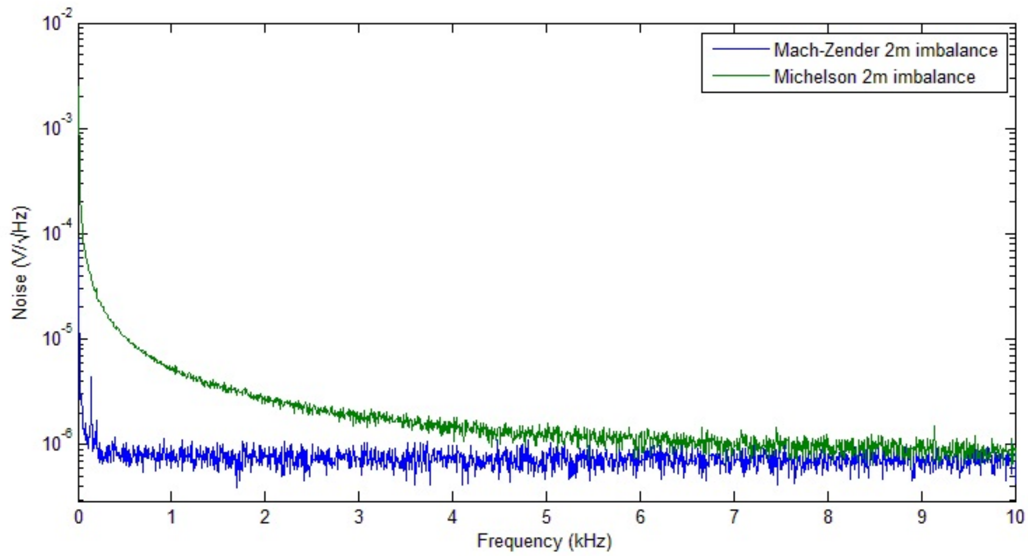

Figure 3.7: Noise Contribution of the Interferometer Type

immune to Rayleigh scattering type of noise sources. But on the other hand, Mach-Zender interferometer has more components and since laser pass through the sensor arms once it has half the sensitivity compared to Michelson interferometer.

Looking at the noise measurements of Mach-Zender and Michelson interferometer setups , we observe similar noise floor levels except the lower frequencies. Michelson interferometer has higher noise level at lower frequencies and this might be the result of the sensitivity of the Michelson interferometer to scattering mechanisms. It can be claimed that Mach-Zender interferometer is more robust than the Michelson interferometer in terms of the noise performance.

Chapter 4

Phase Detection Methods

Interferometric fiber optic detectors are evaluated by measuring phase difference between a reference and sensor arms. Intensities at the output of the interferometer changes with respect to phase difference ($\delta\phi = \phi_s - \phi_r$). Intensity at the output of the interferometer is given as,

$$I_1 = I_s + I_r + 2\sqrt{I_s I_r} cos\left(\delta\phi\right) \tag{4.1}$$

$$I_2 = I_s + I_r - 2\sqrt{I_s I_r} cos\left(\delta\phi\right) \tag{4.2}$$

where I_r and the I_s are the intensities at the reference and sensor arm of the interferometer. A more general representation is given as,

$$I_{1,2} = I_0\left(1 \pm V cos\left(\delta\phi\right)\right) \tag{4.3}$$

where $I_0 = I_r + I_s$ is the average power of the laser source, V is the visibility of the interferometer which is defined as $2\sqrt{I_s I_r}/\left(I_r + I_s\right)$. Output of the interferometer is nonlinearly changes with the phase difference between the arms of the interferometer, cosine term represents the nonlinear relation of phase change to output of the interferometer. [36]

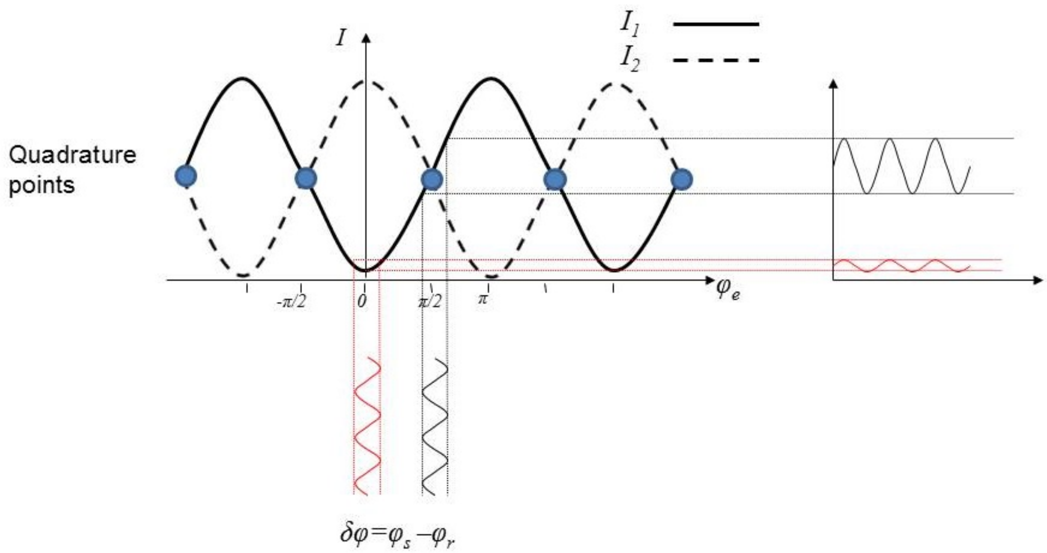

Figure 4.1: Interferometric output with phase bias ϕ_e and small signal phase change $\delta\phi$

Environmental effects have low frequency noise effect on the phase term which can be represented as the phase bias point ϕ_e, this value drifts slowly with time and phase bias point changes by slowly with time. Phase change coming from the difference of the phases of reference and sensor arms can be represented as the small signal phase change $\delta\phi$. When the phase bias is at the odd multiples of $\pi/2$, interferometer is at the quadrature point of phase bias and shows linear response to small signal phase difference $\delta\phi$. When the phase bias is at the multiple values of π cosine term is at either maximum or minimum phase bias point and interferometer exhibits nonlinear behaviour resulting distortion in small signal phase changes.

Environmental effects changes slowly and phase bias moves away from quadrature points to nonlinear points where small signal response is perturbated and signal fading occurs.[37] One method to overcome the signal fading is to use active control of phase bias point by adding a phase compensators to interferometer. [38] Phase compensation is done either with a phase modulator or a piezoelectrically stretched coiled fiber.

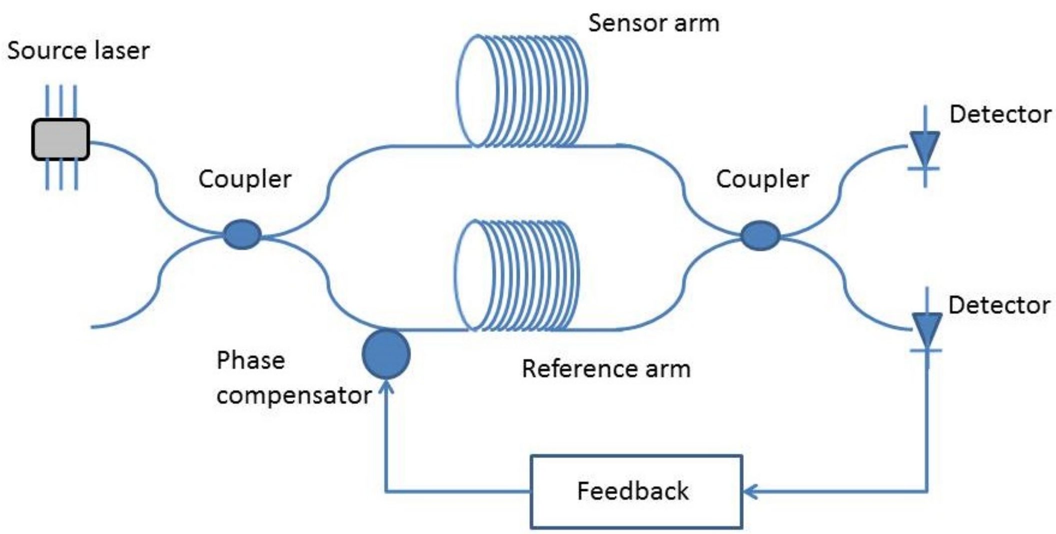

Figure 4.2: Phase compensation in Mach-Zender interferometer

Quadrature phase bias points are when both output of the interferometer is equal. Outputs of the interferometer are $I_1 = I_0 - V cos\,(\delta\phi)$ and $I_1 = I_0 + V cos\,(\delta\phi)$. Differential output of the interferometer is used as error term and a closed loop feedback system is installed to keep the phase bias at the quadrature point. Compensators at the interferometer actively corrects the phase bias by adding phase to one arm of the interferometer. By using compensators low frequency noise stemming from the environmental effects can be corrected and nonlinear perturbation from the output of the interferometric sensor can be eliminated. Highest frequency noise signal that can be corrected is limited with the bandwidth of the closed loop feedback. In order to have a successfull phase detection with phase compensation method, noise frequency and the sensor signal should be separate from each other.

Piezoelectrically stretched fiber coils and phase compensators are bulky and heavier than the sensor itself. Another major disadvantage of compensator method is multiplexing sensor arrays. Since this method is a closed loop system tracking the error term and keeping the phase bias on the quadrature point, when array of sensors are multiplexed compensators for each sensor element must be used and the complexity of the control electronics is multiplied by the sensor number.

4.1 Phase Generated Carrier Method

Phase Generated Carrier (PGC) method is a passive open loop technique. This technique introduces a phase modulation outside the signal bandwidth. Modulation signal carries the signal of interest to sidebands and upconverts them, therefore eliminates the low frequency noise. [39] Light intensity at the output of the interferometer can be written as;

$$I_0 = A + Bcos\left(\theta\left(t\right)\right) \tag{4.4}$$

where, A and B are the constants representing the average intensity and the visibility of the interferometer and $\theta\left(t\right)$ is representing the time varying phase difference between the arms of the interferometer. When a sinusoidal modulation signal with a frequency ω_0 and amplitude C is applied to one arm of the interferometer, intensity at the output of the interferometer becomes,

$$I_0 = A + Bcos\left(Csin\left(\omega_0 t\right) + \phi\left(t\right)\right) \tag{4.5}$$

where the amplitude of the modulation signal C is defined as the modulation depth and ω_0 is the carrier frequency of the PGC method. Carrier signal is generated with a phase modulator or piezoelectrically stretched fiber coil. The signal of interest is represented with $\phi\left(t\right)$. If we expand intensity in terms of

Bessel functions we get,

$$I_0 = A + B\left(\left(J_0\left(t\right) + 2\sum_{k=1}^{\infty}\left(-1\right)^k J_{2k}\left(C\right) cos\left(2k\omega_0 t\right)\right) cos\left(\phi\left(t\right)\right)\right)$$
$$-B\left(\left(2\sum_{k=0}^{\infty}\left(-1\right)^k J_{2k+1}\left(C\right) cos\left(\left(2k+1\right)\omega_0 t\right)\right) sin\phi\left(t\right)\right) \quad (4.6)$$

$$I_0 = A + B\left(\left(J_0(C) + 2J_2(C)cos(2\omega_0 t) + 2J_4(C)cos(4\omega_0 t) + ...\right) cos(\phi(t))\right)$$
$$-B\left(\left(2J_1(C)sin(\omega_0 t) + 2J_3(C)sin(3\omega_0 t) + ...\right) sin(\phi(t))\right) \quad (4.7)$$

where $J_n(C)$ terms are the Bessel functions of the first kind. Intensity of the interferometer is multiplied with $cos(\omega_0 t)$ and $cos(2\omega_0 t)$ functions and first and second harmonic of the carrier signal with its sidebands are downconverted. Downconverted signals are lowpass filtered to eliminate higher harmonics and two baseband signals are generated. [40]

$$L_1 = KJ_1(C)sin(\phi(t)) \quad (4.8)$$

$$L_1 = KJ_2(C)cos(\phi(t)) \quad (4.9)$$

where K is the constant coming from the intensity amplitude. If we set the modulation depth to $C = 2.63$, then coefficients of $cos(\phi(t))$ and $sin(\phi(t))$ becomes equal. J_1=J_2 Phase term $\phi(t)$ can be found by calculating the arctangent of ratio of the baseband signals when $C = 2.63$

$$\phi(t) = tan^{-1}\left(\frac{KJ_1(C)sin(\phi(t))}{KJ_2(C)cos(\phi(t))}\right) = tan^{-1}\left(\frac{sin(\phi(t))}{cos(\phi(t))}\right) \quad (4.10)$$

Downconverted baseband signals give sine and cosine of the interested phase signal. Ratio of the baseband signals equals to the tangent of the phase signal, by calculating the arctangent value phase signal is obtained. [41]

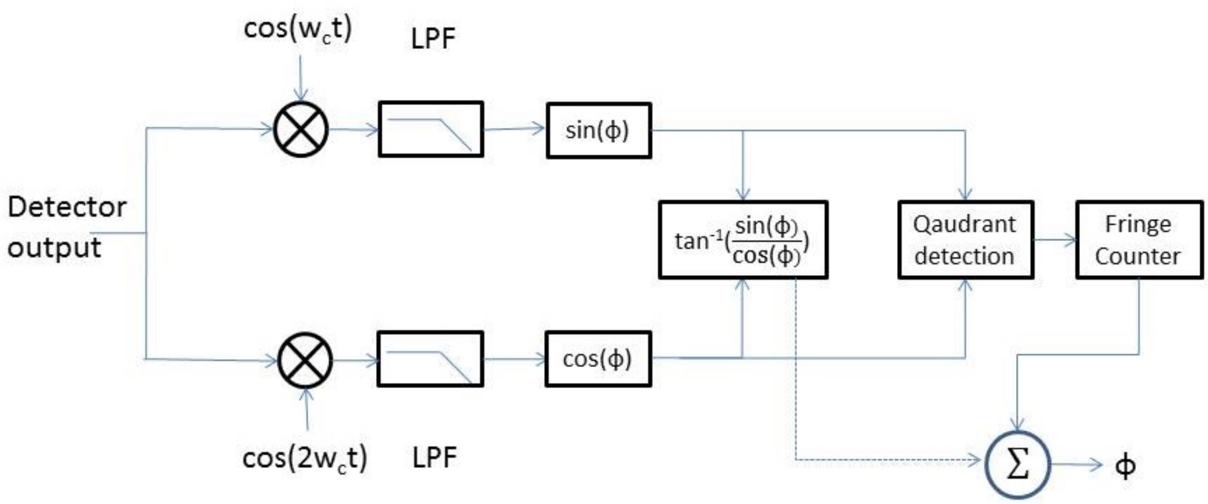

Figure 4.3: Phase Generated Carrier- Arctangent Algorithm

Arctangent operation gives phase values between $-\pi \leq \phi \leq \pi$. When phase signal is larger than π or smaller than $-\pi$, it is wrapped over the unit circle and phase value abrubtly jumps 2π, continuity of the signal is disturbed. Small phase signals are demodulated without distrubting the signal shape, but for large phase signals these abrubt jumps adds extra noise to the detected phase signal. Therefore, dynamic range of the sensor becomes limited by one period of unit circle, 2π.

In order to correct the large phase signals fringe counter is used. Signs of the baseband signals, $sin\,(\phi)$ and $cos\,(\phi)$, are used to find the region of the phase signal and fringe count value is hold in the memory. When implementing the fringe counter, discrete values of $sin\,(\phi[k])$, $cos\,(\phi[k])$ and $sin\,(\phi[k-1])$, $cos\,(\phi[k-1])$

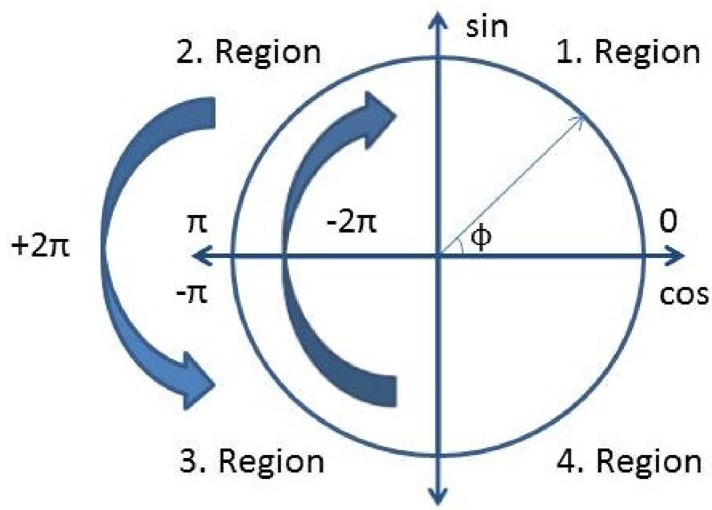

Figure 4.4: Fringe Counting for Correcting Large Phase Signals

are held in the memory, region of the current discrete time and the previous discrete time is calculated. Each time a transition from 2. region to 3. region occurs fringe count value is increased by 2π and each time a transition from 3. region to 2. region occurs fringe count value is decreased by 2π. [42] Fringe count value is added to the output of arctangent function and large signals are unwrapped from the unit circle giving us the true value of the large phase signals. Advantage of using fringe counter is that, dynamic range is increased. Theoretically, dynamic range is increased as much as you can increase the value of fringe count.

I have used MATLAB to evaluate the performance of PGC, output of the interferometer is assumed to be in the form of, $I_0 = A + Bcos\left(Csin\left(\omega_0 t\right) + \phi\left(t\right)\right)$. For testing the performance of PGC method, first a random signal is generated by adding two sine signals at 500Hz and 1400Hz, which demonstrates the signal on the generated by the fiber optic acoustic sensor. Modulation signal at 20kHz is used as the carrier signal, $\omega_0 = 2\pi * 20Khz$, amplitude of the carrier signal is set to C=2.63 rad. PGC arctangent method is used to demodulate the phase signal. As it can be seen from the time domain graphs of demodulated signal and

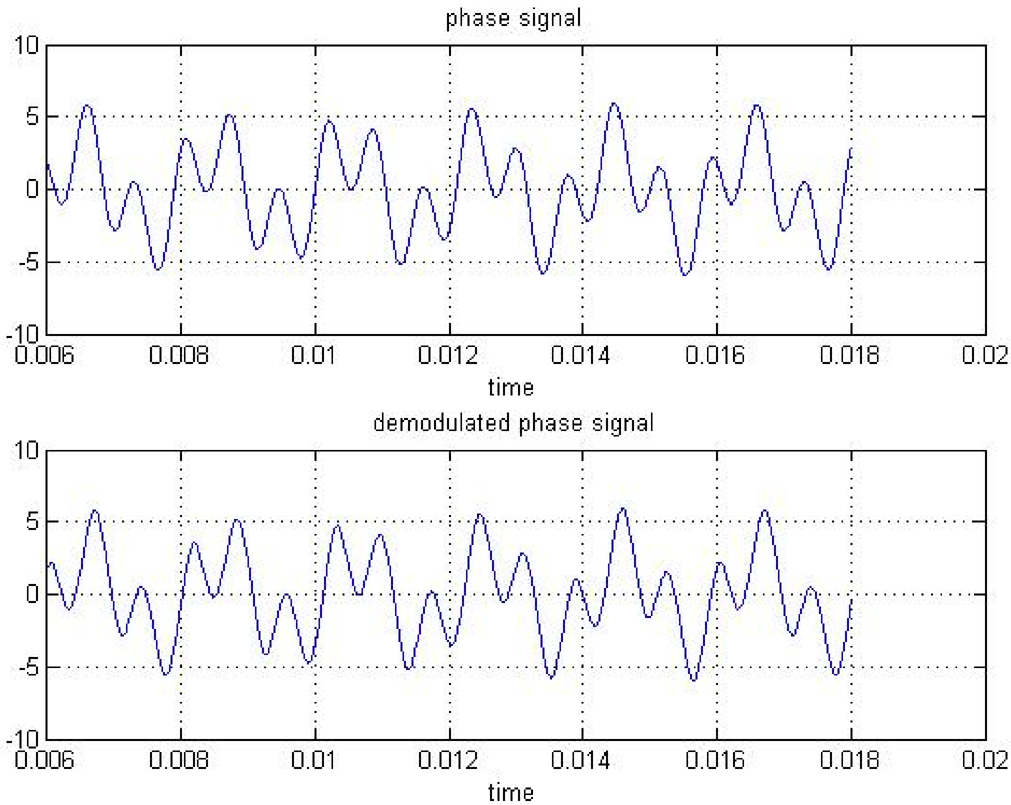

Figure 4.5: Random phase signal and demodulated phase signal with PGC method

the randomly generated signal, randomly generated signal can be demodulated perfectly with PGC method.

There are few key point in PGC method that has to be taken carefully. Carrier signal should be at least two time larger than the highest frequency of interest. Since carrier signal and the second harmonic of the carrier signal is used to demodulate the phase signal. Acoustic signals are upconverted by the carrier signal and its second harmonic signal. If the two times the highest frequency acoustic signal has higher frequency than the carrier frequency, upconverted signals will mix and demodulation will fail. Spectrum of the signal at the output of the detector is shown schematically below.

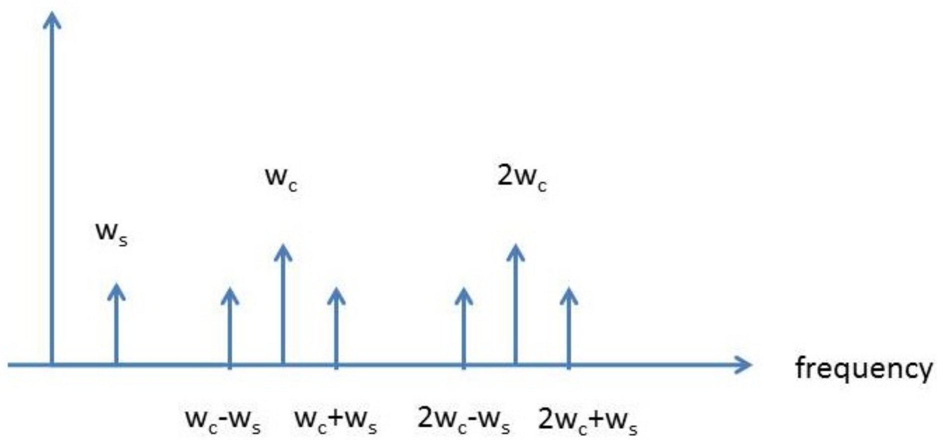

Figure 4.6: Spectrum of detector output

As it can be seen from the spectrum, highest frequency phase signal that can be demodulated is limited by the frequency of the carrier signal. Carrier signal should be at least two times higher than the maximum frequency of interest.

Chapter 5

Ultra Low Noise Fiber Optic Acoustic Sensors for Underwater Applications

Noise is a key parameter when evaluating the performance of an underwater acoustic sensor. In order to detect an acoustic signal at the point of the sensor, signal strength should be higher than the noise sources. For a passive underwater acoustic sensor main noise sources can be defined as ambient noise, self noise of the sensor and vessel noise. Self noise of the sensor is the noise source that is stemming from the sensor itself. Ambient noise is the noise that is coming from the sea and vessel noise is the noise source that occurs from the propellers and propulsion machinery of the platform that is carrying the underwater acoustic sensor. [43, 44] Since the noise source are not correlated with each other, total RMS (root mean square) noise can be calculated by adding squares of the mean noise sources than calculating the square root of the sum.

$$\langle n_{total} \rangle = \sqrt{\langle n_{selfnoise} \rangle^2 + \langle n_{vesselnoise} \rangle^2 + \langle n_{ambientnoise} \rangle^2} \tag{5.1}$$

Passive underwater acoustics sensors are used for listening the acoustic signals

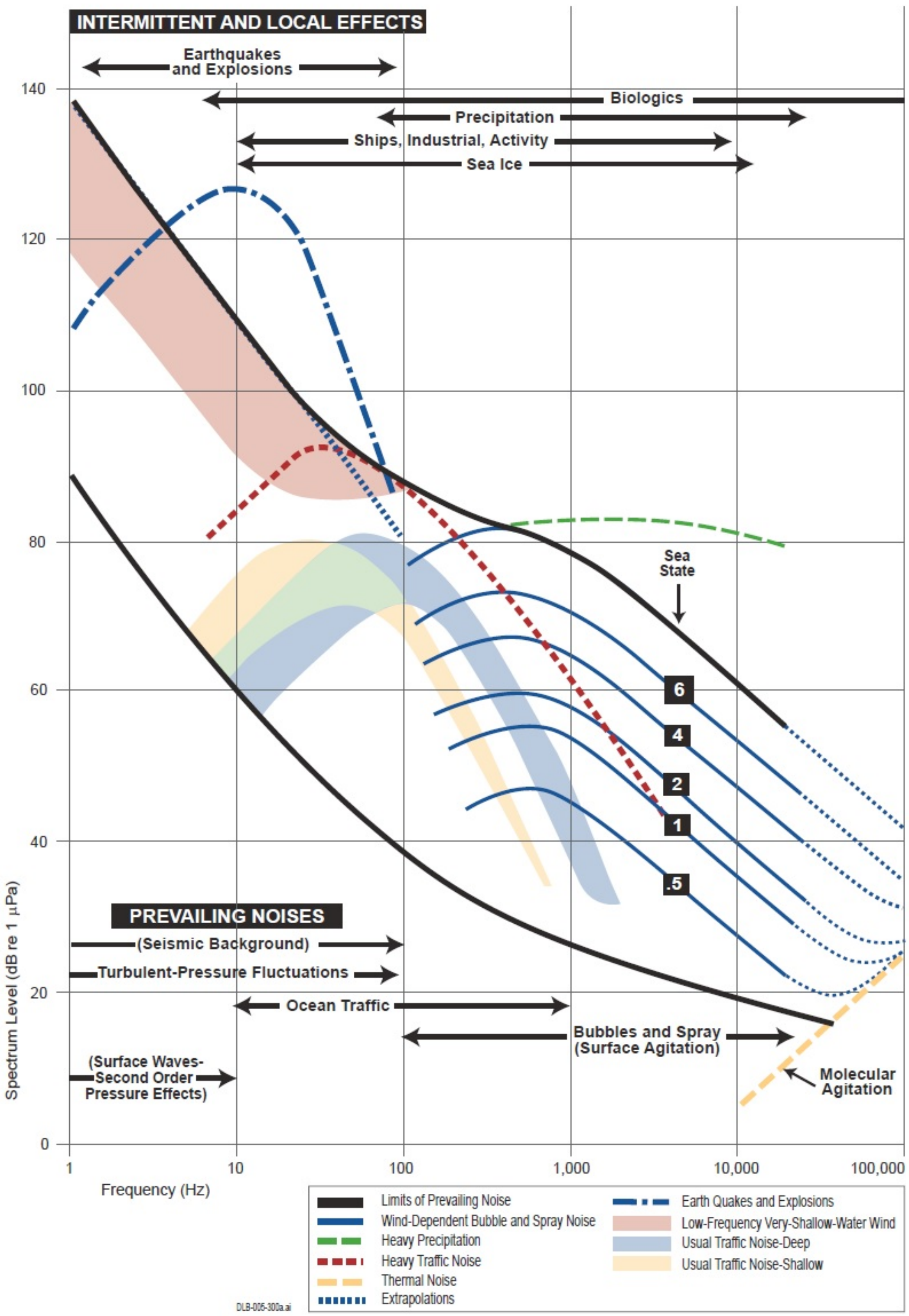

Figure 5.1: Spectral noise levels and noise sources in the ocean

generated by a target. Highest noise source is the one determining the noise level. Self noise of the sensor can be improved by improving the design of the sensor. In order to improve the performance of an underwater acoustic sensor, self noise of the sensor should be lower than the ambient noise of the sea and vessel noise.

Spectral distribution of the ambient noise of the ocean and its sources are shown in the figure. Noise in the ocean is present because of the effects coming from the surface of the sea, seismic noise coming from the bottom of the sea, turbulance and molecular motion inside sea and the living creatures in the sea. Noise contribution from the seismic disturbances coming from the seabed contributes to the low frequency spectrum of the ambient noise. [45]

Table 5.1: Sea state, wind speed and wave height

Sea state	0	1	2	3	4	5	6
Wind speed (knots)	≤ 1	5	13	16	19	22	28
Wave height(m)	0	0.05	0.4	0.7	1.3	2	3

Noise resulting from the surface waves due to wind and waves are dominant above 500Hz. Calm sea without any wind and wave is known as the sea state 0. As the wind speed increases, more wave occur at the surface of the sea and the ambient noise above 500Hz level increases. Sea states, wind speed and wave heights are given in the Table 5.1. [46] Atmospheric events such as wind has a dominant effect on the ambient noise. As the wind speed increases wave heights increase and agitation in the surface increases effecting the ambient noise. Although wind effects the ambient noise of the sea, light rain and light snow does not have significant effect on the ambient noise. We have taken measurements at the Meteksan facilities during rain and snow and we did not observe significant change at the noise level of the Bilkent pond. According to Waite [46], heavy rain can have effect the ambient noise of the sea at all frequencies.

Ship traffic over the ocean also effect the ambient noise of the sea. Propeller of the ships can generate tones at the frequency spectrum, if there is a single ship around it can generate a noise at a very narrow bandwidth of noise but if there are many ships around, combination of the noises generated by all the ships becomes a wide spectrum noise. There is a constant ship traffic over the ocean, which has a contribution to ambient noise level of the sea. Even if there is no ship traffic, no rain or wind or snow, no seismic disturbances, there will be still ambient noise due to molecular motions of the ingredients of sea and the noise due to fishes and plants living in the sea.

Evaluating an underwater acoustic sensor, self noise is good indication of performance, if the self noise of the sensor is higher than the ambient noise, the sensor noise will limit the minimum detectable pressure. If the self noise is better than the ambient noise, minimum detectable pressure will be limited with the ambient noise.

Velocity of an acoustic signal is determined by the properties of the propagation medium such as density ρ and the elasticity modulus E. For fluids compressibility χ is used to calculate the propagation speed of acoustic signal. Compressibility χ is the inverse of elasticity modules E.

$$c = \sqrt{\frac{E}{\rho}} = \sqrt{\frac{1}{\chi\rho}} \tag{5.2}$$

In sea water propagation speed of acoustic signals is approximately c= 1500m/sec, but depending on the depth, pressure, salinity and temperature propagation speed changes. Since the ocean is not an homogenous medium in terms of salinity and temperature, propagation speed changes in the ocean. For example after sunrise water in the sea starts to warm up from the surface and density of the water changes from surface to down, which leads to a gradient of propagation speed.

Acoustic signals are characterized by the frequency of the signal. Frequency of the acoustic signal is the number of vibrations per second. Wavelength of the acoustic signal is the spatial change during the period T, or it is the distance that the acoustic signal propagates during a period T. For example, an acoustic signal at 10 kHz has wavelength of 15 cm but an acoustic signal at 100 Hz has wavelength at 15 m.

$$\lambda = cT = \frac{c}{f} \tag{5.3}$$

Frequency of the acoustic signal also effects the attenuation of the signal, size of the acoustic signal generators, target acoustic response. Frequency of the signal determines the size of the wavelength, if the target is smaller than the wavelength of the acoustic signal reflected energy gets smaller. Therefore, a specific target can reflect more energy at smaller wavelengths. Acoustic signal generators becomes larger as the frequency of the acoustic signal gets smaller.

Table 5.2: Frequency, wavelength and maximum usable range

Frequency	Wavelength	Maximum usable range
100 Hz	15 m	1000 km
1 kHz	1.5 m	100 km
10 kHz	15 cm	10 km
100 kHz	1.5 cm	1 km
1000 kHz	1.5 mm	0.1 km

Acoustic signals experience propagation loss as the signal travels through the medium. Propagation loss can be divided into two parts, geometrical spreading loss, absorbtion loss. Geometrical spreading loss is occurs, when the signal source behaves like a point source. As the source spreads and signal propagates, signal energy at the surface of the wavefront decreases. Other source of propagation loss is the absorbtion losses. Absorptions losses comes from the viscosity of water, chemical reactions. Absorbtion losses depends on the salinity, temperature, depth and frequency. There are mathematical models for calculating the absorbtion losses, but in a general manner to get a sense of the absorbtion we can say that the absorbtion loss increases as the frequency increases. We can say that lower frequency acoustic signal experience less absorbtion loss and can propagate longer distances before the signal power drops lower than noise floor of the sea. Frequency band of the acoustic sensor also determines the area of usage. [47]

Some of the areas of usage of the acoustic spectrum is given in Table 5.3. Fiber optic acoustic sensor designed in Meteksan has detection bandwidth from 250 Hz to 5 kHz, fiber optic acoustic sensors don't have capability to generate acoustic

Table 5.3: General usage of sound spectrum

Frequency Range	Main Acoustic Systems
0.1- 1 kHz	Seismic Exploration
1 - 10 kHz	Sediment Profilers
20 - 1000 kHz	Doopler current profilers
20 - 500 kHz	Fishery echo sounders and sonars
0.01 - 10 kHz	Passive military sonars
0.2 - 20 kHz	Active military sonars
5 - 100 kHz	Transmission and positioning
100 - 1000 kHz	Sidescan sonars
150 kHz -	Medical Ultrasound

signal, they are passive systems. Therefore, looking at the general areas of usage, designed fiber optic acoustic sensor can be used in seismic explorations, passive military sonars. It can also be used in active military sonar by coupling fiber optic acoustic sensors with an acoustic signal generator. Another area of usage for fiber optic acoustic hydrophones is all fiber optic vector sensors. There are experimental works on all fiber optic vector sensors. [48] Fiber optic hydrophones are integrated with fiber optic accelerometers and all fiber optic vector sensors are built. Attractive property of the fiber optic sensors is that instead of using lots of electrical cables, vector sensors can be interrogated with two fiber cables, without EMI/EMC problems.

Another attractive point of fiber optics acoustic sensors is that sensors can be easily multiplexed and all the array elements can be interrogated from the same fiber optic cable. Array of fiber optic acoustic sensors are used as towed arrays and towed arrays are used for beamforming. Detected acoustic signal's direction can be found by processing the data coming from the array elements. [49, 50, 51]

Besides the military applications, fiber optic acoustic sensor designed can be used in the oil and gas industry for following the seismic events happening in the reservoir of the oil or gas extraction sites below the ocean. Because arrays can be formed with many hydrophone element, sensor cables spanning large areas can be constructed. Also, fiber optic solutions for monitoring the seismic events under the ocean, are more robust than the electrical counterparts since the wet end is in all fiber and the electrical parts such as interrogators, laser drivers are isolated from water. There are successful examples of fiber optic acoustic sensors used in reservoir monitoring.[52, 53, 54]

After evaluating the possible areas of usage for the fiber optic acoustic sensor designed, performance of the sensor will be evaluated. First noise performance of the fiber optic acoustic sensor will be evaluated. Noise measurement setup is given below.

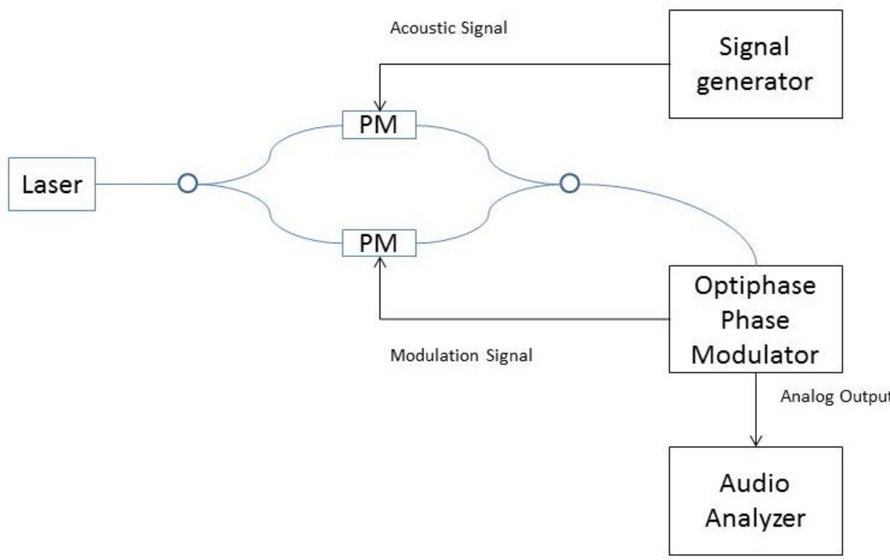

Figure 5.2: Noise Measurement Setup

Since the electronic card that will be used to interrogate the fiber optic acoustic sensor is not completed, noise measurement are taken with OPD4000 optical phase modulator of Optiphase company. OPD4000 uses phase generated carrier method to demodulate the phase signal. Rest of the noise measurement setup is used to emulate the fiber optic acoustic sensor system. Noise measurement setup is designed as close as possible to the actual design of the sensor system to reflect the real performance. Fiber optic part of the measurement setup is seen in Figure 5.3. After laser input, an isolator is added to protect the laser source from backreflections. Variable optical attenuator is used to adjust the power level used in the noise measurement setup. Two coupler is used to install the Mach-Zender interferometer and phase modulator are added to both arms of the interferometer. Phase modulator in one arm of the Mach-Zender interferometer is used to add the carrier signal used in PGC method and the other phase modulator is used to emulate the phase shift that will come from the fiber optic acoustic prob of the sensor system. Laser source of the setup is PS-NLL laser with 5kHz. Imbalance of the Mach-Zender interferometer is set to less than one meter. PGC demodulation is done with 20 kHz carrier signal. Carrier signal is generated by OPD4000 phase demodulator.

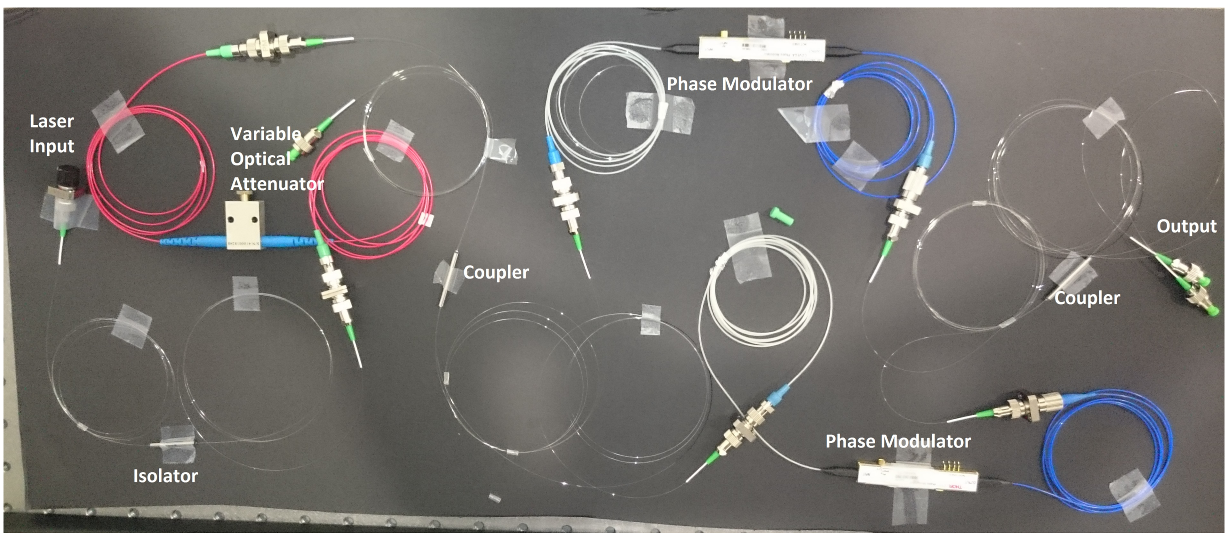

Figure 5.3: Picture of the Noise Measurement Setup

Noise measurement is done in terms of radians to determine the system noise performance, than by using the measured responsivity of the fiber optic acoustic probe noise unit is converted into pressure units and it is evaluated against the noise levels of the ocean. Responsivity of the designed fiber optic acoustic probe is -140 dB re rad/μPa and this value is used to convert noise level. Unit conversion is done as given in the equation below.

$$MinimumDetectablePressure\left(\mu Pa/\sqrt{Hz}\right) = \frac{SystemNoiseLevel\left(rad/\sqrt{Hz}\right)}{Responsivity\left(rad/\mu Pa\right)} \quad (5.4)$$

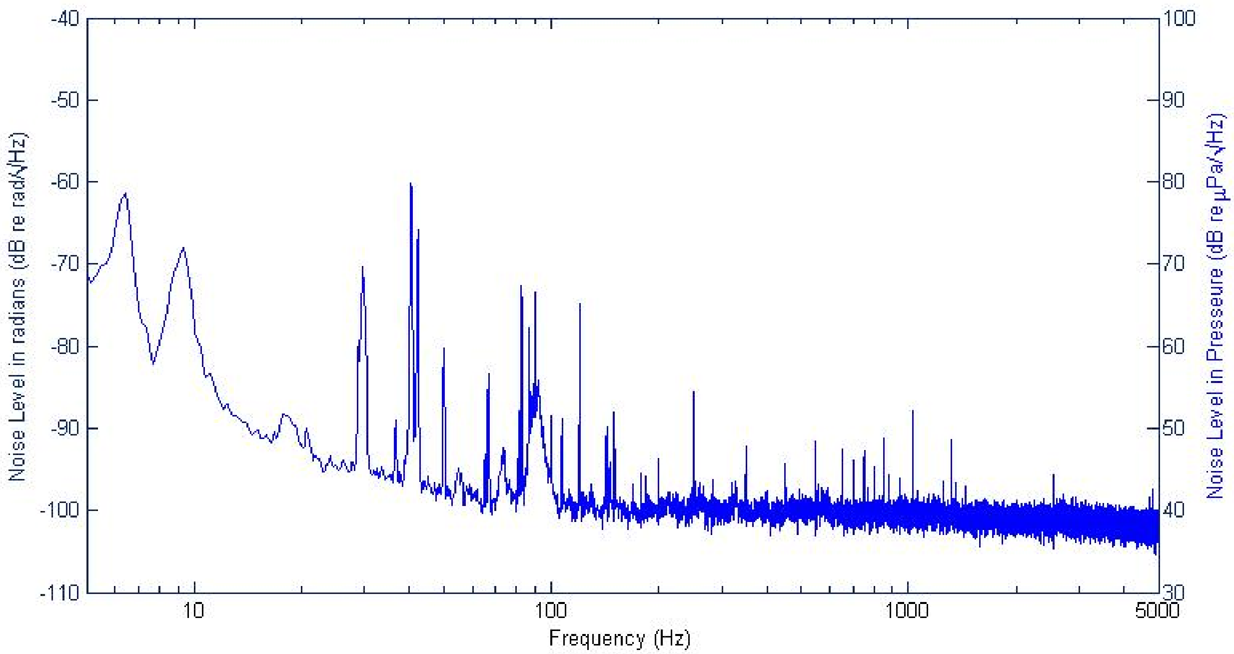

Figure 5.4: Noise Level of the Designed Fiber Optic Acoustics

Measured noise level is given in Figure 5.4. Measurement is done in the lab environment, therefore there are peaks in the spectrum which comes from the environment. Left axis of the measurement is the noise density in terms of radians and right axis of the measurement is the noise density in terms of pressure. Noise level above 100 Hz is close to 40 dB re $\mu Pa/\sqrt{Hz}$ which is close to sea state zero of the ocean noise. Sea state zero is the state where there is no wind or wave and no shipping traffic noise. It is almost impossible to find such state of the ocean. Therefore, it is safe to say that noise level of the designed sensor is lower than the ambient noise of the ocean. Contribution of the self noise of the fiber optic acoustic sensor is negligible compared to the contribution of the ambient noise. Acoustic signal detection by the designed fiber optic acoustic sensor is limited by the ambient noise of the ocean. Improving the noise level further to lower levels will not improve the performance of signal detection, because the ambient noise is limiting the signal detection.

After measuring the noise level of the fiber optic acoustic sensor, phase change with different amplitudes are applied at 1 kHz with the phase modulator which emulates the fiber optic acoustic probe. By changing the amplitude of the phase shift with phase modulator, demodulated phase amplitudes from the audio analyzer is recorded. In order to calculate the percentage linearity absolute value of the percentage error is subtracted from 100. Percentage linearity is calculated as below.

$$Linearity(\%) = 100 - \frac{Abs(ActualValue - DetectedValue) * 100}{ActualValue} \quad (5.5)$$

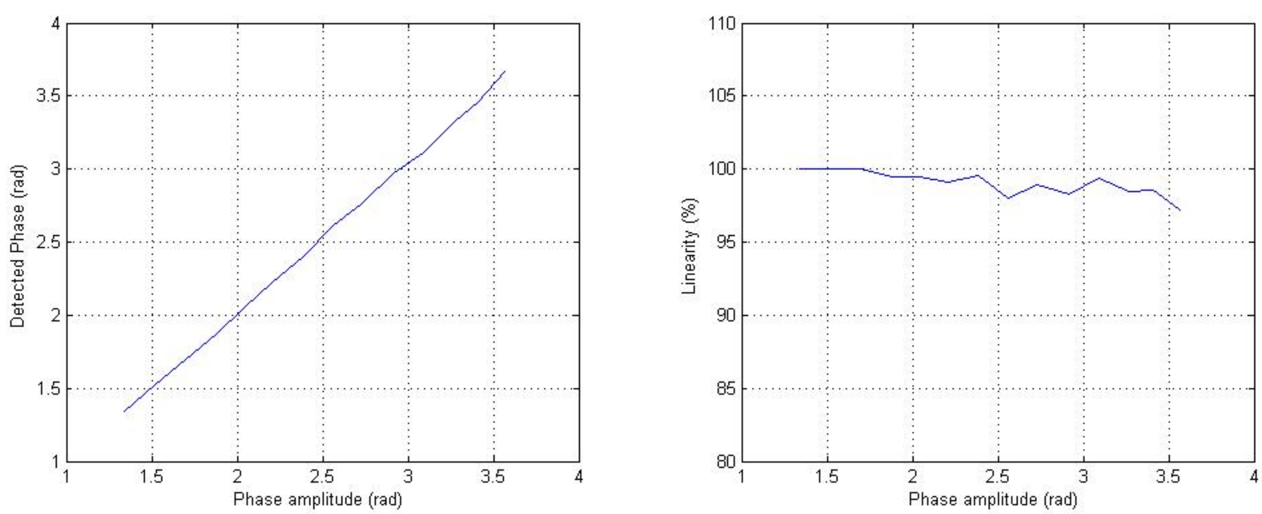

Figure 5.5: Phase amplitude linearity

As the amplitude of the phase shift is changed, we observe from the measurements that linearity of the sensor stays over 97 percents. Phase shift will occur when the acoustic signal is detected by the fiber optic acoustic probe. As the amplitude of the acoustic signal increases, detected signal stays linear.

Linearity of the fiber optic acoustic sensor in frequency is tested by changing the frequency of the phase signal given from the phase modulator emulating

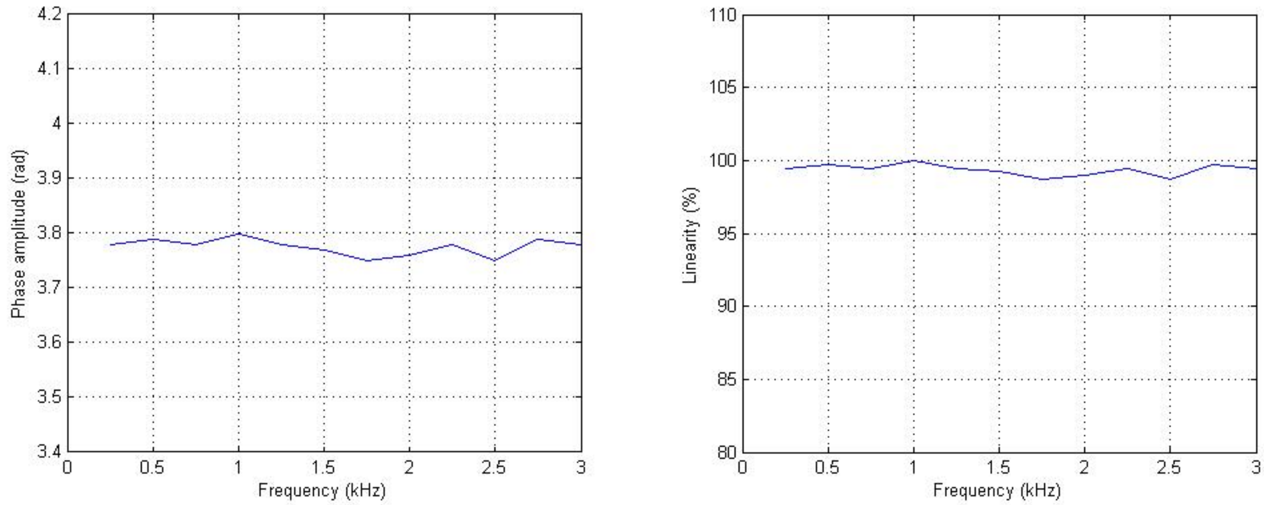

Figure 5.6: Phase amplitude linearity with frequency change

the fiber optic acoustic probe. Phase signal with amplitude 3.8 rad is applied at different frequencies and percentage linearity of the detected phase signal is calculated. Percentage linearity of the acoustic signal from 250 Hz to 3 kHz is above 98 percent.

Chapter 6

Conclusion

Fiber optic sensor have many advantages over the counter technology sensors, such as EMI immunity, low weight, flexible geometric design, no electrical connection at the remote sensing point. Fiber optic sensor are being used in many areas. Acoustic sensing, strain sensing, temperature sensing, magnetic field sensing, rotation sensing, chemical/biomedical sensing are main areas where fiber optic sensor are being used.

In this thesis, mandrel type fiber optic acoustic underwater sensors are analyzed in terms of their noise performance. Experimental work and simulation have been done to evaluate the design parameters of the mandrel type fiber optic acoustic sensors.

In order to emulate fiber optic acoustic sensor experimental setups are constructed and experiments to analyze noise performance characteristics have been done. Experiments have shown us that using a high quality laser source, which has low phase noise and low RIN value, lowers the noise of the interferometer. Experimental results also have shown us that imbalance of the interferometer increases the noise level at the output of the interferometer. Interferometer type used in the design of the mandrel type fiber optic sensor also effects the noise at the output of the interferometer. Mach-Zender type interferometer have lower noise level at lower frequencies compared to Michelson type of interferometers. Photodetector used at the design of the fiber optic sensor also effects the noise performance of the sensor. Lower NEP value detector gives lower noise floor but responsivity of the photodetector is also important in terms of power budget of the laser source. When using a lower responsivity photodetector laser power should be increased in order to get meaningful voltage values at the output of the detector. Therefore choosing a detector with a lower NEP value and higher responsivity will be best solution for both noise performance of the sensor and power budget of the laser source.

Performance of the fiber optic acoustic sensor is evaluated by it noise performance, dynamic range and responsivity. Responsivity of the sensor is determined by mechanical design of the mandrel, fiber length used on the sensor. Dynamic range of the sensor is determined by the maximum and minimum acoustic signal that can be detected. PGC method used to demodulate the phase change of the interferometer has very large dynamic range because of fringe counting property. Noise level of the fiber optic acoustic sensor should be compared with the environmental noise of the medium it will be used. Ambient noise of the ocean is effected by various effects. Noise levels are defined with sea states which defines the noise level in different climatic conditions.

Noise level of the design is measured by using commercial product since the electronic cards is not completed. While measuring the noise level an experimental setup is installed to emulate the design. Low phase noise laser is used with Mach-Zender interferometer, and the path imbalance of the interferometer is set to less than one meter. Measured noise level about -100 dB rad/$\sqrt{Hz}$ above 100 Hz. Using the responsivity of the noise level measured in terms of radians converted to pressure units. Responsivity of the designed sensor is -140 dB re rad/μPa, which gives noise level about 40 dB re μPa/$\sqrt{Hz}$ noise level. This noise level is equal to the noise level of the ocean at sea state zero (SS0). Sea state zero is the level when there is no wind, wave or shipping traffic noise. Therefore any signal above the ambient noise level of the ocean can be detected with the designed fiber optic acoustic sensor. Noise level of the designed sensor is lower than the ambient noise of the ocean, which means signal detection is not limited with the sensor noise but it is limited with the ambient noise of the ocean. Finally, linearity of the sensor against amplitude and frequency is tested and measurement have shown the linearity is over 97 percent for both frequency change and amplitude change.

Bibliography

[1] A. D. Kersey, "A review of recent developments in fiber optic sensor technology," *Optical Fiber Technology*, vol. 2, no. 3, pp. 291 – 317, 1996.

[2] K. Kuang, R. Kenny, M. Whelan, W. Cantwell, and P. Chalker, "Embedded fibre bragg grating sensors in advanced composite materials," *Composites Science and Technology*, vol. 61, no. 10, pp. 1379–1387, 2001.

[3] X. Pan, D. Liang, and D. Li, "Optical fiber sensor layer embedded in smart composite material and structure," *Smart materials and structures*, vol. 15, no. 5, p. 1231, 2006.

[4] S. Melle, K. Liu, *et al.*, "Wavelength demodulated bragg grating fiber optic sensing systems for addressing smart structure critical issues," *Smart Materials and Structures*, vol. 1, no. 1, p. 36, 1992.

[5] R. Maaskant, T. Alavie, R. Measures, G. Tadros, S. Rizkalla, and A. Guha-Thakurta, "Fiber-optic bragg grating sensors for bridge monitoring," *Cement and Concrete Composites*, vol. 19, no. 1, pp. 21–33, 1997.

[6] A. D. Kersey, "Optical fiber sensors for permanent downwell monitoring applications in the oil and gas industry," *IEICE transactions on electronics*, vol. 83, no. 3, pp. 400–404, 2000.

[7] G. Shiach, A. Nolan, S. McAvoy, D. McStay, C. Prel, and M. Smith, "Advanced feed-through systems for in-well optical fibre sensing," in *Journal of Physics: Conference Series*, vol. 76, p. 012066, IOP Publishing, 2007.

[8] T. Yamate, "Fiber optic sensors for the exploration of oil and gas," in *19th International Conference on Optical Fibre Sensors*, pp. 700438–700438, International Society for Optics and Photonics, 2008.

[9] J. Dakin, C. Wade, and M. Henning, "Novel optical fibre hydrophone array using a single laser source and detector," *Electronics Letters*, vol. 20, no. 1, pp. 53–54, 1984.

[10] S. Goodman, S. Foster, J. Van Velzen, and H. Mendis, "Field demonstration of a dfb fibre laser hydrophone seabed array in jervis bay, australia," in *20th International Conference on Optical Fibre Sensors*, pp. 75034L–75034L, International Society for Optics and Photonics, 2009.

[11] D. Tosi, M. Olivero, and G. Perrone, "Low-cost fiber bragg grating vibroacoustic sensor for voice and heartbeat detection," *Applied optics*, vol. 47, no. 28, pp. 5123–5129, 2008.

[12] J. Dorighi, S. Krishnaswamy, and J. D. Achenbach, "Response of an embedded fiber optic ultrasound sensor," *The Journal of the Acoustical Society of America*, vol. 101, no. 1, pp. 257–263, 1997.

[13] P. Morris, P. Beard, and A. Hurrell, "Development of a 50 mhz optical fibre hydrophone for the characterisation of medical ultrasound fields," in *Proc. IEEE Ultrasonics Symp*, vol. 9, pp. 1747–1750, 2005.

[14] J. Deng, H. Xiao, W. Huo, M. Luo, R. May, A. Wang, and Y. Liu, "Optical fiber sensor-based detection of partial discharges in power transformers," *Optics & Laser Technology*, vol. 33, no. 5, pp. 305–311, 2001.

[15] G. Yilmaz and S. E. Karlik, "A distributed optical fiber sensor for temperature detection in power cables," *Sensors and Actuators A: Physical*, vol. 125, no. 2, pp. 148–155, 2006.

[16] M. Niklès, B. H. Vogel, F. Briffod, S. Grosswig, F. Sauser, S. Luebbecke, A. Bals, and T. Pfeiffer, "Leakage detection using fiber optics distributed temperature monitoring," in *Smart Structures and Materials*, pp. 18–25, International Society for Optics and Photonics, 2004.

[17] B. Vogel, C. Cassens, A. Graupner, and A. Trostel, "Leakage detection systems by using distributed fiber optical temperature measurement," in *SPIE's 8th Annual International Symposium on Smart Structures and Materials*, pp. 23–34, International Society for Optics and Photonics, 2001.

[18] D. Inaudi and B. Glisic, "Long-range pipeline monitoring by distributed fiber optic sensing," *Journal of pressure vessel technology*, vol. 132, no. 1, p. 011701, 2010.

[19] B. Culshaw, G. Stewart, F. Dong, C. Tandy, and D. Moodie, "Fibre optic techniques for remote spectroscopic methane detectionfrom concept to system realisation," *Sensors and actuators B: chemical*, vol. 51, no. 1, pp. 25–37, 1998.

[20] W. Cao and Y. Duan, "Optical fiber-based evanescent ammonia sensor," *Sensors and Actuators B: Chemical*, vol. 110, no. 2, pp. 252–259, 2005.

[21] R. Jorgenson and S. Yee, "A fiber-optic chemical sensor based on surface plasmon resonance," *Sensors and Actuators B: Chemical*, vol. 12, no. 3, pp. 213–220, 1993.

[22] S. Oho, H. Kajioka, and T. Sasayama, "Optical fiber gyroscope for automotive navigation," *Vehicular Technology, IEEE Transactions on*, vol. 44, no. 3, pp. 698–705, 1995.

[23] E. Udd and W. B. Spillman Jr, *Fiber optic sensors: an introduction for engineers and scientists*. John Wiley & Sons, 2011.

[24] O. Çelikel, "Construction and characterization of interferometric fiber optic gyroscope (ifog) with erbium doped fiber amplifier (edfa)," *Optical and quantum electronics*, vol. 39, no. 2, pp. 147–156, 2007.

[25] A. Stockbridge, "Fiber optic hydrophones (april 2011),"

[26] J. De Freitas, "Recent developments in seismic seabed oil reservoir monitoring applications using fibre-optic sensing networks," *Measurement Science and Technology*, vol. 22, no. 5, p. 052001, 2011.

[27] D. Hill and P. Nash, "Fiber-optic hydrophone array for acoustic surveillance in the littoral," in *Defense and Security*, pp. 1–10, International Society for Optics and Photonics, 2005.

[28] J. H. Cole, C. Kirkendall, A. Dandridge, G. Cogdell, and T. Giallorenzi, "Twenty-five years of interferometric fiber optic acoustic sensors at the naval research laboratory," in *Washington Academy of Sciences*, vol. 90, pp. 40–57, 2004.

[29] G. Wild and S. Hinckley, "Acousto-ultrasonic optical fiber sensors: overview and state-of-the-art," *Sensors Journal, IEEE*, vol. 8, no. 7, pp. 1184–1193, 2008.

[30] C. D. Butter and G. Hocker, "Fiber optic strain gauge," *Fiber Optics Weekly Update*, p. 245, 1978.

[31] J.-i. Im and Y. Roh, "A finite element analysis of an interferometric optical fiber hydrophone with a concentric composite mandrel including a foaming layer," *The Journal of the Acoustical Society of America*, vol. 106, no. 3, pp. 1363–1368, 1999.

[32] K. Yin, M. Zhang, T. Ding, L. Wang, Z. Jing, and Y. Liao, "An investigation of a fiber-optic air-backed mandrel hydrophone," *Optics Communications*, vol. 281, no. 1, pp. 94–101, 2008.

[33] M. C. Teich and B. Saleh, "Fundamentals of photonics," *Canada, Wiley Interscience*, p. 3, 1991.

[34] R. Paschotta, "Noise in laser technology," *Optik & Photonik*, vol. 4, no. 2, pp. 48–50, 2009.

[35] B. Moslehi, "Noise power spectra of optical two-beam interferometers induced by the laser phase noise," *Lightwave Technology, Journal of*, vol. 4, no. 11, pp. 1704–1710, 1986.

[36] C. Kirkendall, "Overview of high performance fiber optic sensing," in *Lasers and Electro-Optics, 2002. CLEO'02. Technical Digest. Summaries of Papers Presented at the*, pp. 393–vol, IEEE, 2002.

[37] S. K. Sheem, T. G. Giallorenzi, and K. Koo, "Optical techniques to solve the signal fading problem in fiber interferometers," *Applied Optics*, vol. 21, no. 4, pp. 689–693, 1982.

[38] D. Jackson, R. Priest, A. Dandridge, and A. B. Tveten, "Elimination of drift in a single-mode optical fiber interferometer using a piezoelectrically stretched coiled fiber," *Applied Optics*, vol. 19, no. 17, pp. 2926–2929, 1980.

[39] A. Dandridge, A. B. Tveten, and T. G. Giallorenzi, "Homodyne demodulation scheme for fiber optic sensors using phase generated carrier," *Microwave Theory and Techniques, IEEE Transactions on*, vol. 30, no. 10, pp. 1635–1641, 1982.

[40] T. R. Christian, P. A. Frank, and B. H. Houston, "Real-time analog and digital demodulator for interferometric fiber optic sensors," in *1994 North American Conference on Smart Structures and Materials*, pp. 324–336, International Society for Optics and Photonics, 1994.

[41] J. Bush, A. Cekorich, and C. K. Kirkendall, "Multichannel interferometric demodulator," in *Third Pacific Northwest Fiber Optic Sensor Workshop*, pp. 19–29, International Society for Optics and Photonics, 1997.

[42] A. Cekorich, "Demodulator for interferometric sensors," in *SPIE Photonics East*, vol. 99, pp. 3860–50, 1999.

[43] J. U. Robert, "Principles of underwater sound," *New York: McGraw-Hill Book Company*, 1983.

[44] R. J. Urick, "Ambient noise in the sea," tech. rep., DTIC Document, 1984.

[45] D. Bradley and R. Stern, "Underwater sound and the marine mammal acoustic environment: A guide to fundamental principles," *US Marine Mammal Commission.(12 December 2011*, 2008.

[46] A. D. Waite and A. Waite, *Sonar for practising engineers*, vol. 3. Wiley London, 2002.

[47] X. Lurton, *An introduction to underwater acoustics: principles and applications*. Springer Science & Business Media, 2002.

[48] J. Wang, H. Luo, Z. Meng, and Y. Hu, "Experimental research of an all-polarization-maintaining optical fiber vector hydrophone," *Journal of Lightwave Technology*, vol. 30, no. 8, pp. 1178–1184, 2012.

[49] Z. Meng, Y. Hu, M. Ni, S. Xiong, R. Zhang, X. Li, G. Stewart, F. Dong, and B. Culshaw, "Development of a 32-element fiber optic hydrophone system," in *Optics East*, pp. 114–119, International Society for Optics and Photonics, 2004.

[50] W. Zhang, F. Li, and Y. Liu, "Field test of an eight-element fiber laser hydrophone array," in *OFS2012 22nd International Conference on Optical Fiber Sensor*, pp. 8421AX–8421AX, International Society for Optics and Photonics, 2012.

[51] C. Kirkendall, T. Barock, A. Tveten, and A. Dandridge, "Fiber optic towed arrays," tech. rep., DTIC Document, 2007.

[52] J. Langhammer-Optoplan, "A step towards the optical oil field,"

[53] J. T. Kringlebotn, H. Nakstad, and M. Eriksrud, "Fibre optic ocean bottom seismic cable system: from innovation to commercial success," in *Proc. SPIE*, vol. 7503, pp. 75037U–1, 2009.

[54] J. Langhammer, H. Nakstad, M. Eriksrud, A. Berg, E. Ronnekleiv, O. H. Waagaard, M. Thompson, *et al.*, "Fibre optic reservoir monitoring: field trials and results," in *Offshore Technology Conference*, Offshore Technology Conference, 2008.

Appendix A

Code

A.1 PGC arctangent method

```
clear;
    f_sampling= 500000;
    dt=1/(f_sampling);
    NFFT=4*8192;
    t=[dt:dt:NFFT*dt];
    fs=500; % frequency of the acoustic signal
    fp=20000; % frequency of the PGC carrier signal
    A=1; B=1; C=2.62; D=3;
    %phase signal which will be demodulated
    teta= D*(sin(2*pi*fs*t)+sin(2*pi*1400*t));
```

```
%signal at the output of the detector

intensity= A+B*cos(C*cos(2*pi*fp*t)+teta);

% downconversion

j1=intensity.*cos(2*pi*fp*(t-1));

j2=intensity.*cos(2*2*pi*fp*(t-1));

% calculating the filter coefficients

wc1=fp/(2*f_sampling);

[b1,a1]=butter(5,wc1,'low');

%filtered jacobians

jf1=filter(b1,a1,j1);

jf2=filter(b1,a1,j2);

%arctangent calculation

arctangent=atan(jf1./jf2);

%finding the region of the angle

bolge=j1;

for i=1:length(jf1)

if(sign(jf1(i))==1)

if(sign(jf2(i))==1)

bolge(i)=1;
```

```
arctangent(i)= arctangent(i)-pi; else

bolge(i)=2;

arctangent(i)= arctangent(i);

end

else

if(sign(jf2(i))==1)

bolge(i)=4;

arctangent(i)= pi+ arctangent(i);

else

bolge(i)=3;

arctangent(i)= arctangent(i);

end

end

end

phi=arctangent;

%fringe counting

fr_count=0;

for j=2:length(jf1)

if (bolge(j-1)-bolge(j))== 3
```

fr_count=fr_count+1; end

if bolge(j-1)-bolge(j)== -3

fr_count=fr_count-1; end

phi(j)=arctangent(j)+2*pi*fr_count;

end

figure(1) subplot(2,1,1) plot(t(3000:9000),teta(3000:9000)) xlabel(’time’) title(’phase signal’) grid on

subplot(2,1,2) plot(t(3000:9000),phi(3000:9000)) xlabel(’time’)

title(’demodulated phase signal’)

grid on

wc1=8000/(2*f_sampling); [b,a]=butter(5,wc1,’low’); phi=filter(b,a,phi);

j1_fft=fft((j1),NFFT)/NFFT;

j2_fft=fft((j2),NFFT)/NFFT;

intensity_fft=fft((intensity),NFFT)/NFFT; teta_fft=fft((teta),NFFT)/NFFT; phi_fft=fft((phi),NFFT)/NFFT; arctangent_fft=fft((arctangent),NFFT)/NFFT;

f = f_sampling/2*linspace(0,1,NFFT/2+1);

figure(2);

plot(f/1000,2*abs(phi_fft(1:NFFT/2+1)),f/1000,2*abs(teta_fft(1:NFFT/2+1))) xlabel(’frekans (kHz)’);